

**UNIVERSITY OF LISBON
FACULTY OF SCIENCES
PHYSICS DEPARTMENT**



NEW SCINTILLATORS FOR NUCLEAR MEDICINE

**MASTER THESIS
Rui Gonalo Azinheiro**

**INTEGRATED MASTER’S IN BIOMEDICAL ENGINEERING AND
BIOPHYSICS -
CLINICAL ENGINEERING AND MEDICAL INSTRUMENTATION
2013**

**UNIVERSITY OF LISBON
FACULTY OF SCIENCES
PHYSICS DEPARTMENT**



NEW SCINTILLATORS FOR NUCLEAR MEDICINE

**MASTER THESIS
Rui Gonalo Azinheiro**

**INTEGRATED MASTER’S IN BIOMEDICAL ENGINEERING AND
BIOPHYSICS -
CLINICAL ENGINEERING AND MEDICAL INSTRUMENTATION**

**Supervisor in Philips Research: Dr. Herfried Wiczorek
Internal Supervisor: Dr. Pedro Almeida**

2013

“A journey is best measured in friends, not in miles.”

- *Tim Cahill*

AKNOWLEDGEMENTS

My first big thank you will go to Herfried Wiczorek for giving me this great opportunity and experience, and also for his availability, advising, trust and guiding during these 8 months and also for the help in the thesis. I also want to thank very much to the whole team that participated in the scintillator project while I was there for helping me with everything that I needed. Another acknowledgement goes to everybody on the department for welcoming me there. Here a special thank you to Odette and Wilma our amazing secretaries.

I also want to thank to Pedro Almeida, my supervisor in the University for the Availability and the help through this process and through all the help during these 6 years in during the course. I also want to thank all the teachers that were with me during all of these years especially to Eduardo Ducla Soares.

Going back to Philips, I also want to thank a lot, really a lot, to Pedro and Andreia for being my Portuguese comrades of all the time in the cold Eindhoven, remembering me that there is always a place where the sky is blue and the Sun actually “works”. This thank you is also for all the professional help and I thank even more the help teaching me the ways of the Dutch.

A big thank you, also, to my Portuguese friends of all time for supporting me every time that I needed. I also want to thank them for all the support during my university years, here a special note for my Lisbon friends: you made all of these years easy.

Now, a very very special thank you to my family! Always there for everything that I need, always supportive, always together.

Last but not least, I want to thank and dedicate this work to my Eindhoven friends. You were like a family during these months! You made everything special, you made Eindhoven enjoyable and most of all unforgettable. This thank you is specially directed to Giulia, Johan, Sahil, Ale, Maureen, Ricardo, Paki; to the best housemates: Fons, Mehdi, Yan and Sandra. And of course, my last special thank you is to Chiara, the best gift that Eindhoven gave me.

RESUMO

Um equipamento de Tomografia por Emissão de Positrões (PET) é um equipamento utilizado em imagiologia médica que recorre à introdução de radiofármacos que emitam positrões, no interior do corpo do paciente. Os positrões são rapidamente aniquilados quando em contacto com electrões, emitindo neste processo dois fotões com uma energia de 511 keV (radiação- γ) que viajam em direcções opostas e serão detectados no anel de detectores presente dos equipamentos de PET. O percurso realizado por cada par de fotões é denominado linha de resposta (LoR). É a informação de múltiplas LoR que permitem a reconstrução e obtenção da imagem em PET. Os radiofármacos utilizados apresentam características semelhantes à glucose, permitindo assim o seu alojamento e consequente detecção em locais onde o metabolismo é mais elevado. O elevado metabolismo está frequentemente associado a doenças oncológicas, sendo esta a principal utilização do equipamento de PET.

Actualmente os equipamentos de PET mais modernos utilizam, em conjunto com a LoR, a informação do tempo de voo de cada um dos fotões, originado assim os *scanners* de *Time of Flight* (TOF) PET. A utilização do tempo de voo é realizada através da diferença de tempo registada entre a detecção de cada fotão no anel de detectores. Essa diferença de tempo é posteriormente utilizada para calcular a posição da aniquilação através da fórmula: $\Delta x = c(t_1 - t_2)/2$. As vantagens da utilização de TOF PET são a redução do ruído e uma maior precisão na imagem. O uso da informação do tempo de voo permite também a redução da dose de radionuclídeo utilizada em cada exame, já que para a reconstrução da imagem são necessárias menos contagens. Este facto leva também a que o tempo de exame menor.

A principal diferença entre um equipamento de PET convencional e um equipamento TOF PET encontra-se nos detectores utilizados, sendo cada um destes detectores constituído por um cintilador e por um fotodetector. O cintilador tem a função de converter a radiação proveniente do paciente em radiação visível que será posteriormente detectada e convertida num sinal mensurável no fotodetector.

Os desafios da utilização de TOF PET prendem-se com a resolução temporal dos detectores. Os detectores utilizados hoje em dia possuem uma resolução temporal de ~ 500 ps, o que equivale a uma resolução espacial de ~ 7.5 cm. Esta resolução espacial está longe de permitir que um *scanner* utilize exclusivamente a informação do tempo de voo num exame, sendo portanto necessário incluir esta informação nos métodos de reconstrução convencionais, para gera assim uma imagem melhor. Para além desta característica, os cintiladores utilizados em PET são muito caros.

O trabalho realizado na Philips Research Eindhoven teve como objectivo encontrar novos cintiladores que apresentassem uma eficiência tão próxima quanto possível dos cintiladores utilizados hoje em dia em *Time of Flight* (TOF) PET e que apresentassem um custo de produção mais baixo. Para termos de comparação de resultados foram utilizados os cristais de LYSO, presentes nos sistemas da Philips e os cristais produzidos por uma empresa concorrente, os Furukawa.

Nesta investigação foram utilizados cintiladores cerâmicos, em contraponto aos cristais únicos utilizados hoje em dia nos sistemas de PET (LYSO, GSO e LSO). A grande diferença entre estes dois tipos de cintiladores é a estrutura, já que um cristal único apresenta uma estrutura cristalina única e uma cerâmica/*garnet* é o resultado de uma agregação de várias estruturas microscristalinas. No entanto o princípio de acção de ambos é semelhante.

Os testes realizados incluíram dois tipos diferentes de medições, com diferentes fotodetectores. O primeiro tipo de medições era efectuado em PMTs à temperatura ambiente. As medições nos PMTs eram efectuadas para avaliar o tempo de decaimento de cada cristal/disco/pó, já que foram feitas análises aos três estágios das cerâmicas para tentar avaliar a relação existente entre eles. Para uma maior eficácia na análise dos resultados foi inserido o cálculo do tempo de decaimento efectivo ($\tau_{eff} = N_{PMT}/U_{PMT}(0)$). Este parâmetro foi também utilizado para estimar os valores de CRT de cada cristal medido. O outro tipo de medições realizado foi realizado com arrays de 8x8 cristais em acoplados a um fotodetector digital de silicone, sendo que os anel exterior do *array* era constituído por duas filas de cristais de LYSO e no centro eram colocados os *garnets* que se pretendiam medir. Em ambos os casos as medições foram realizadas em coincidência para que fossem reproduzidas as condições encontradas num *scanner* real. As medições com os d-SiPMs foram realizadas numa câmara climática a 5°C para otimizar a eficiência do detector. Esta temperatura mais baixa não devia afectar o desempenho do cintilador. A principal diferença entre um PMT e um d-SiPM é a digitalização do sinal logo após a detecção que ocorre no segundo detector. Isto permite que o sinal possa ser lido mais rápido e com um menor ruído devido à utilização de *trigger levels* que permite eliminar contagens aleatórias (*Dark counts*) que ocorram durante a aquisição do sinal. Um outro mecanismo utilizado para melhorar o sinal destes fotodetectores é a realização de um *dark count map*, que bloqueia a aquisição das contagens das células do detector que contenham um maior número de contagens aleatórias.

As medições com PMTs permitiram também identificar a presença em todas as amostras de componentes lentas de decaimento/*afterglow*. No entanto para estimar o valor de

CRT foi utilizada apenas a primeira componente de decaimento, já que esta é a que mais contribui para o valor absoluto deste parâmetro.

A principal diferença entre os *garnets* que foram medidos era a sua composição. A principal diferença entre as amostras deu-se ao nível da composição dos *garnets*. Estas alterações incidiram essencialmente na concentração de Ga (entre 2 e 3 mol) e de Ce (entre 0.2 e 1.2% em proporção à concentração de Ga), já que as componentes de Al e Gd desempenhavam principalmente funções estruturais e o Lu foi utilizado devido à sua elevada absorção.

Os resultados obtidos demonstraram uma grande influência da concentração de Ga na CRT dos cintadores, verificando-se que com o aumento da concentração de Ga, tanto o tempo de decaimento, como o CRT diminuía, verificando-se assim a dependência que o CR tem em relação ao tempo de decaimento. Os valores de CRT observados variaram entre 572 e os 1502ps, sendo os melhores valores de CRT obtidos com [Ga]=3 e os piores com [Ga]=2. Esta diminuição era também acompanhada por uma diminuição do LO, que variaram entre 500 e os 2000 fotões ópticos. Esta diminuição veio também demonstrar a relação existente entre o LO e dE/E. Quanto maior o LO, maior o dE/E. Em relação ao aumento da concentração de Ce verificou-se que quanto maior esta fosse, menor seria o CRT, no entanto este efeito não é tão evidente como o efeito da concentração de Ga.

Os principais problemas observados nos *garnets* correspondiam à presença de um elevado *afterglow*, bem como à falta de transparência de algumas amostras, que pode ser em parte explicada pelo método pouco industrializado utilizado na sua construção.

Simultaneamente com o estudo do efeito da composição dos *garnets* foi também testada uma teoria para estimar os valores de CRT verificando-se que apesar de algumas discrepâncias a tendência geral das medições está de acordo com a literatura.

Considerando os resultados obtidos pode considerar-se que o objectivo de encontrar um *garnet* que pudesse substituir os cintiladores actualmente utilizados foi alcançado, apesar de ainda ser necessária alguma investigação num contexto mais industrializado.

Palavras chave: Time of Flight PET, fotão, garnet, LYSO, detector

ABSTRACT

The use TOF PET brings some challenges to the medical industry, since these scanners require that the scintillators used have a specific set of characteristics, but most of all they need to be fast (low coincidence resolving (CRT) and low decay time) and as less expensive as possible. In this context lately the research had been focusing on ways to introduce ceramics in this field. The focus of this work was the study of changing the concentration of some components in ceramics built using Lu, Ce, Ga, Al and Gd. The measurements were made using PMTs to measure the decay time in powders/disks/single crystals and d-SiPMs to measure CRT, Light Output (LO) and energy resolution (dE/E) arrays built with LYSO and garnets. In the PMTs it was observed the presence of a slow component in the decay time in every sample. To precisely measure decay time it was introduced the effective decay time: $\tau_{eff} = N_{PMT}/U_{PMT}(0)$. The values of τ_{eff} were between ~70 and 210ns, being the decay time lower with higher [Ga]. In d-SiPM it was verified that the higher the amount of Ga the lower is the CRT and the lower is the LO. The values of CRT were between 572 and 1502ps, and the LO between 500 and 2000 optical photons. The tradeoff presents a future challenge since it compromises the dE/E of the ceramic. The change in Ce was similar to the one verified in Ga. The other elements have mainly structural purposes.

Time of Flight PET, photon, garnet, LYSO, Detector

CONTENTS

1. INTRODUCTION	1
2. PHYSICAL PRINCIPLES OF NUCLEAR IMAGING	3
2.1. PHYSICS OF NUCLEAR MEDICINE IMAGING	3
2.1.1. γ -ray emission.....	3
2.1.2. β^+ decay.....	4
2.1. FROM ANGER CAMERA TO PET	5
2.1.1. Anger camera and SPECT.....	5
2.1.2. PET.....	6
3. SCINTILLATORS FOR PET AND SPECT.....	12
3.1. INORGANIC SCINTILLATORS IN MEDICAL IMAGING.....	12
3.1.1. The LYSO scintillator.....	18
3.2. PHOTODETECTORS♦.....	19
3.2.1. PMT	19
3.2.2. Digital Silicon Photomultipliers.....	20
Sensor architecture and characteristics	21
4. EXPERIMENTAL METHODS.....	25
4.1. PMT MEASUREMENTS.....	25
4.1.1. PMT measurements: Analysis.....	27
4.2. PHILIPS PDPC TEK MEASUREMENTS	27
4.2.1. Preparation of the array for TEK measurements	29
5. RESULTS	30
5.1. PMT RESULTS	30
5.1.1. Results from powders:.....	32
Results from disks	32
Results from sticks	34
5.2. TEK RESULTS	35
Overview of TEK results.....	36
6. DISCUSSION.....	43
7. CONCLUSIONS AND FUTURE WORK.....	47
8. REFERENCES	48

TABLE INDEX

<i>Table 1: Physical and Scintillation properties of some scintillators [12]</i>	<i>18</i>
<i>Table 2: Resume of the logic involved in the trigger levels of the Philips D-SiPM sensor, as well as the average number of photons necessary to activate each trigger level. In the table sp1, 2, 3 or 4 stand for each sub-pixel in the die. [22].....</i>	<i>22</i>
<i>Table 3: General characteristic of the d.SiPM used in this project.[23].....</i>	<i>24</i>
<i>Table 4: Resume of the settings used in the PMT measurements.</i>	<i>26</i>
<i>Table 5: Settings used for the TEK measurements.....</i>	<i>28</i>
<i>Table 6: Overview of the relevant results achieved for the sample in which the rise time was measured.....</i>	<i>42</i>

FIGURE INDEX

Figure 1: Schematic diagram of a conventional gamma camera used in SPECT. [7]	5
Figure 2: Left Example of the SPECT scanner, Brightview that belong to Philips portfolio of nuclear medicine imaging equipment. In this scanner it is possible to see two gamma cameras used for the acquisitions. [26]	
Right: example of the image that it is possible to obtain using the Brightview scanner using Tc-99m.[27]	6
Figure 3: Schematic explaining the differences in the acquisition using Time of Flight and a regular PET scanner. [28]	7
Figure 4: Example of the image that is possible to get in a PET scanner. On the left is the image of a common scanner and on the right is the image of a TOF scanner. On that image it is possible to observe the lower noise level. [29]	9
Figure 5: The four types of events that can be detected in a PET scanner. True events corresponding to the true detection of both photons that arise from the same annihilation and don't suffer any kind of scattering. Randoms which is the detection of two photons that come from different annihilations but are detected in the same LOR. There is also the scattering coincidence which can give rise to a false line of response. The last type of even that can be detected is the spurious coincidence which is another false coincidence originated by a random photon from another part of the body. [30]	10
Figure 6: Example of the shape of the signal obtained in a detector.	10
Figure 7: Example of a Philips Gemini, a PET CT scanner commercialized nowadays by Philips. [31]	11
Figure 8: Example of a state of the arte PET detector used in the Gemini TF system. In each module LYSO crystals are glued to a light guide and readout by a set of PMTs. The module offers a CRT time resolution of 480 ps (new generation) up to 590 ps (second generation). [32]	12
Figure 9: Schematic of the type of scintillators available.	13
Figure 10: Schematic of the production of light in a scintillator [14]	14
Figure 11: Energy band structure of an activated crystalline scintillator. [33]	16
Figure 12: Selection of the best elements for being the best host materials for gamma ray measurements based on the following criteria: toxicity, Energy gap, easy growth and intrinsic radioactivity. [11]	17
Figure 13: Components of a PMT. [19]	20
Figure 14: Example of Philips D-SiPM [23]	21
Figure 15: Schematic of the validation method that occurs in Philips d-SiPMs. [22]	23
Figure 16: On the left Histogram of a dark count map at different temperatures. [21] On the right: a typical distribution of the PDE of Philips PDPC D-SiPM sensor. [23]	24
Figure 17: Schematic of the PMT measurements.	25
Figure 18: On the left, an example of the vikuity case used to measure the sticks. On the right: an example of the plastic disks containing the powders.	26
Figure 19: Schematic of the arrays used (top view). The white squares represent the LYSO crystals and the yellowish ones represent the garnets.	28

Figure 20: Comparison of the signal obtained from different scintillators: Garnet 165-3 (black), LYSO (red) and Furukawa (Blue).	30
Figure 21: Graphic showing the effects of using different fits to get the values of the decay times. For comparison is also shown the value of the effective decay time for the same sample.....	31
Figure 22: Trend of the effective decay time according to different concentration of cerium and gallium on sticks. Settings used in the acquisition: trigger 1 and 2 = -80mV; overall acquisition time = 20 μ s.....	31
Figure 23: 2-D plot showing the effect of the Ga content in the decay time The linear fit was used only as a figure to show the general trend.....	32
Figure 24: Graphics with the trends of decay time and effective decay time according to different concentration of Gallium and Cerium on powders.....	32
Figure 25: Trend of the effective decay time according to different concentration of cerium and gallium on disks. Settings used in the acquisition: trigger 1 and 2 = -80mV; overall acquisition time = 20 μ s.	33
Figure 26: Trend of the decay time according to different concentration of cerium and gallium on disks. Settings used in the acquisition: trigger 1 and 2 = -80mV; overall acquisition time = 20 μ s.....	33
Figure 27: Trends showed by the PMT measurements on sticks.	34
Figure 28: Example of the graphics obtained with Matlab for one of the arrays measured. The two outside layers are made with LYSO. The core is built with four different garnets, following the schematic presented before. From left to right, top to bottom there is: The counts, the CRT, the energy resolution and the number of photons. On top there is the schematic of the disposition of the crystals in the array.....	35
Figure 29: Overview of the CRT values of some of the samples measured. The lowest value achieved still belongs to LYSO, but some of the garnets were able to surpass the values of Furukawa. The four samples inside the circle are the ones that present better CRT values than the LYSO.....	36
Figure 30: Overview of the LO values our garnets.	37
Figure 31: Overview of the dEE results.	37
Figure 32: Overview of the number of counts normalized to the number of counts of the LYSO.....	38
Figure 33: CRT behavior in garnets according to the concentration of Ga.	39
Figure 34: Trend of the LO with Ce and Ga content.....	39
Figure 35: Relation between effective tau and CRT.....	40
Figure 36: shows an overview of CRT measurements and results of this theory. Blue upward triangles show results for trigger level 1, purple downward triangles for trigger level 2, while the magenta triangles give the results of our CRT theory.....	40
Figure 37: Relation between Energy resolution and the number of photons.	41

1. INTRODUCTION

Nuclear Medicine Imaging has acquired a great importance in medical diagnosis in the last decades. These techniques, that started with the Anger camera and have later lead to the introduction of SPECT, PET/CT and PET/MR systems, assume great importance in the detection of most of physiological disorders of the Human organism, including the detection of Cancer, a disease that affects a significant number of people, especially in the Developed Countries as the life span increases, nowadays.

The most advanced type of nuclear medicine scanner used nowadays is the PET scanner. Due to its full ring of detectors that can detect coincidences in time, a much better precision and signal to noise ratio in the detection of lesions than the other nuclear medicine scanners, namely, SPECT, is obtained. Recently in the field of PET scanners it has been introduced a type of scanners that use the Time of Flight (TOF) of gamma radiation to detect the position of a lesion within a few centimeters uncertain in the Line-Of-Response (LOR). TOF acts as “sensitivity multiplier” allowing using lower dose of the radionuclide for the same noise, or if the same dose is used to obtain images with less noise and smaller acquisition times than the conventional scanners. This leads to significant improvements in the clinical patient workflow and lesion detectability. One of the main problems with the TOF scanners used nowadays is the high cost that they represent, being the materials used in the detectors one of the main responsible for those high costs. In this context, Philips started a project in which I participated and based my thesis.

The aim of my internship at Philips Research that led to this thesis was to characterize ceramic garnets with different compositions to enable optimized performance for Time of Flight PET. These ceramic garnets should have a cost/benefit ratio compatible with the scintillators that are used nowadays. This project was developed with a team in Philips Research, in Eindhoven, the Netherlands in a period of almost 8 months in which were measured several samples with different compositions in order to find the best combination in order to get the best CRT results.

To introduce the reader to the work done, the thesis will start with a general introduction to nuclear medicine in the first chapter. In this chapter it will be explained all the physics involved in the nuclear medicine imaging field, as well as the evolution of the scanners used, starting with the gamma camera and finishing with Time of Flight PET.

The second chapter will focus mostly on the parts of the detector used in PET scanners: photodetectors and scintillators, presenting some of the principles involved in these

parts, as well as a literature review that helps to understand the materials used in the ceramics in this project.

The third chapter will explain the methods used to make all the measurements and analysis of the samples studied.

Following the methods there will be presented the most relevant results achieved, which are related with the behavior of the ceramics according to their compositions. After the results there will be a discussion, which will include all the formulas used to calculate all the theory results presented.

The last chapter of this thesis will include a brief resume of all the conclusions achieved as well as some indications for future work.

2. PHYSICAL PRINCIPLES OF NUCLEAR IMAGING

Nuclear medicine is the field of medical sciences that uses radioactive tracers for diagnostic and therapeutic purposes. The main difference between nuclear medicine and other imaging techniques that use radiation, like X-rays, is that in nuclear medicine, the radioactive source is located inside the subject of study which allows obtaining *in vivo* metabolic images of the body using radio-isotopes with specific tropism. These radio-isotopes can be injected, breathed in or swallowed. Due to their biochemical properties they will be distributed with an increased uptake in tissues with high metabolism, e.g. tumors increasing the emission of radiation in these regions of the body. This emission happens due to the decay of the radionuclides, which leads to the emission of high energy photons with a high probability of escaping the body and consequently being detected.

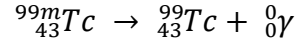
In nuclear medicine imaging there are various types of scanners, which include: the gamma (Anger) camera, Single Photon Emission Computed Tomography (SPECT) and Position Emission Tomography (PET). Both SPECT and PET systems can be combined with anatomic imaging modalities like CT and MR. All of them had as a basis the detection of particles emitted by radionuclides. [1][2]

2.1. Physics of nuclear medicine imaging

Radionuclides are isotopes that undergo into spontaneous nuclear transformation. Almost all of the heavy elements in the periodic table are radioactive, and the majority of the radioactive isotopes is man-made. All these radionuclides decay under one of the following types of decay: α , $\beta^{(+,-)}$ or γ , being the β^+ and γ the most important types of decay to nuclear medicine imaging. The γ -ray emission is the type of decay needed for SPECT, in other hand, due to the need to detect coincidences, in PET it is necessary to use a radionuclide that emits positrons, and in consequence two photons that will allow to measure coincidences. [3], [4]

2.1.1. γ -ray emission

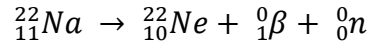
A γ -ray emission is an emission characteristic from excited nuclei. The transition from the excited state to the ground state leaves Z and A unchanged. The most common γ -ray emission nucleus used in nuclear medicine is $^{99m}_{43}\text{Tc}$, which has a half-life of 6.02h, making it perfectly suitable for SPECT scanners. The equation that shows this decay is:



The energy of the γ -ray emitted is 140eV.[5]

2.1.2. β^+ decay

The other type of decay useful in nuclear medicine is the β^+ decay, which is the type of decay that has as result the emission of a positively charged electron, called positron, and a neutrino (ν). This is the decay that is the basis of Positron Emission Tomography (PET). One of the nuclei that present this decay is ${}^{22}_{11}\text{Na}$ (Radionuclei used in all the experiments performed to measure the γ decay). This decay is shown in the following equation:



This type of decay leaves a change in the mass number of the nuclei. The energy released in this decay is given by the mass difference between the parent nucleus and the daughter nucleus, being the mass of the parent is bigger than the mass of the daughter. Considering the specific decay of ${}^{22}_{11}\text{Na}$ the energy released in decay is given by the following equations:

$$Q = M_{Na,N} - M_{Ne,N} - m$$

Expressing the previous equation in atomic masses ($M_{Na,A}$ & $M_{Ne,A}$), and considering that Na has 11 electrons and Ne 10, we get:

$$\begin{aligned} Q &= M_{Na,N} + 11m - (M_{Ne,N} + 10m) - 2m \\ &= M_{Na,A} - M_{Ne,A} - 2m \end{aligned}$$

Considering now the change in the masses of parents (ΔP) and daughters (ΔD) we get that the energy released in any positron decay is:

$$Q_{\beta^+} = \Delta P - \Delta D - 2mc^2$$

By this equation is possible to know that in order to have a β^+ decay the mass of the parent must be larger than the mass of the daughter, with a difference of at least 1022MeV. This amount of energy, present in a positron will be released after its annihilation in contact with matter, originating in two photons with 511keV that will travel in opposite directions.

This process presents all the important properties that are advantageous for imaging and lead directly to the concept of PET.

- 1- The annihilation photons are very energetic (γ -ray region of the electromagnetic spectrum), giving them have a high probability of escaping the body for external detection. [1]

- 2- The two photons are emitted with a precise geometric relationship. If both photons can be detected and localized externally, the line joining the detected locations passes directly through the point of annihilation. This line is called the line of response – LOR (Figure 3). This was originally referred to as electronic collimation. Because the point of annihilation is very close to the point of positron emission, this also gives a good indication of where the radioactive atom was in the body. [1]

The most important radionuclides for PET imaging are fluorine-18 and carbon-11. Particularly, the ^{18}F labeled glucose derivative 2-deoxy-2- ^{18}F fluoro-Dglucose (^{18}F FDG) represents the most widely used PET radiopharmaceutical which has contributed most to the worldwide success of clinical PET imaging. The combination of a highly efficient radiochemistry and a high yielding $^{18}\text{O}(\text{p},\text{n})^{18}\text{F}$ nuclear reaction makes ^{18}F FDG available in large amounts and also enables shipment and distribution by commercial users.[6]

2.1.From Anger camera to PET

The first type of nuclear scanner to appear was the Anger Camera, followed by Single Photon Emission Computed Tomography (SPECT) and later by Positron Emission Tomography (PET).

2.1.1. Anger camera and SPECT

The Anger camera is the basic unit of detection in a SPECT scanner. This type of scanner is used only to detect single events, unlike the PET systems that detect coincidences. This fact makes the image reconstruction easier, even though, it also reduces the quality of the information that we can get from one scanner and the quality of the same.

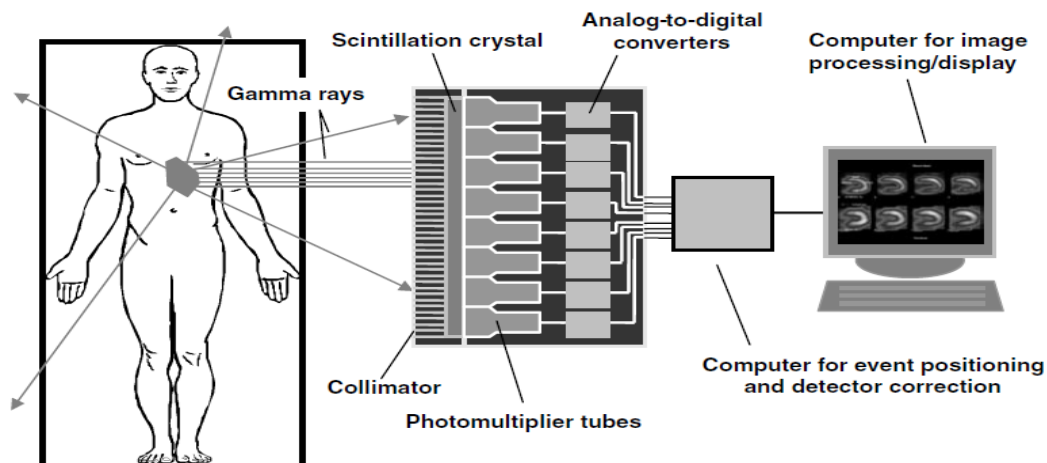


Figure 1: Schematic diagram of a conventional gamma camera used in SPECT. [7]

The Anger camera is the simplest of the nuclear medicine imaging equipment. It consists of: photodetectors (usually PMTs), a scintillator and a collimator.[7]

The main goal of a gamma camera is to detect only the gamma rays that successfully traverse the collimator. As soon as this happens the gamma ray finds the first element of detection, called a scintillator, a material responsible to produce light through the absorption of high energy gamma photons. The light will thereby be collected in a photodetector (photomultiplier) that will produce an electric signal, which will be converted into a digital signal that will be reconstructed into an image. The collimator in the gamma camera has the main function to absorb all the γ -rays that don't travel in a parallel direction of its septa. In the image this will reflect in a reduction of noise and avoid the detection of photons that aren't originated in the region of interest.

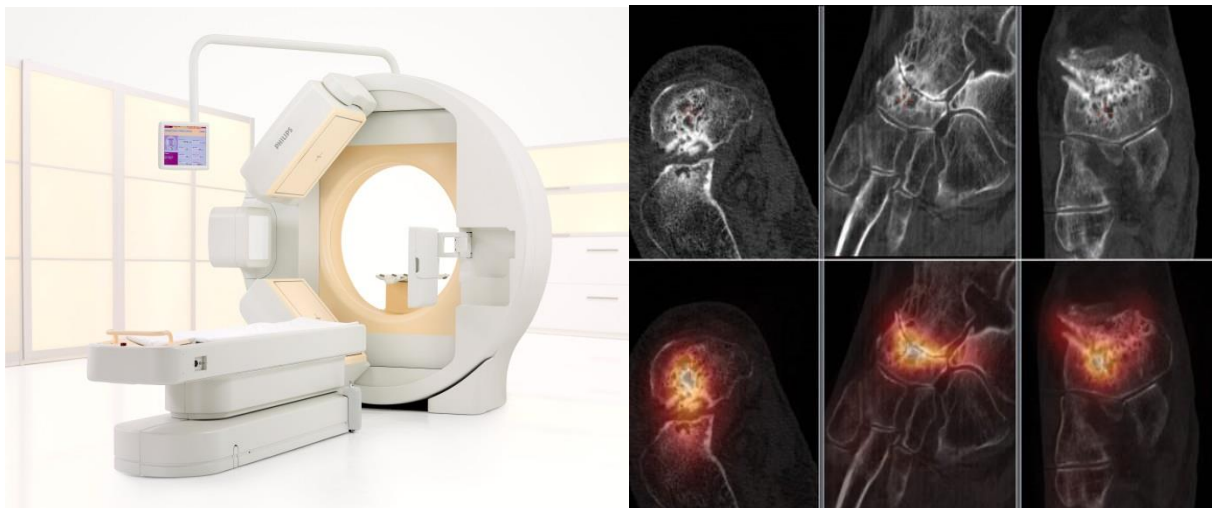


Figure 2: Left Example of the SPECT scanner, Brightview that belong to Philips portfolio of nuclear medicine imaging equipment. In this scanner it is possible to see two gamma cameras used for the acquisitions. [26] Right: example of the image that it is possible to obtain using the Brightview scanner using Tc-99m.[27]

In a SPECT scanner the acquisition is tomographic, meaning that the signal is measured from several points of view, positioning the camera at many orientations around the patient. A common SPECT scanner has more than one camera installed giving the possibility to acquire multiple projection images simultaneously, decreasing the amount of time needed to perform the scan as well as the dose of radionuclide necessary to perform the full scan of the patient.

The most commonly used SPECT radionuclides are Technetium- (^{99m}Tc) and Iodine-123 (^{123}I), with half-lives of 6.02 h and 13.2 h, respectively. [6]

2.1.2. PET

The main difference between a Positron Emission Tomography and the SPECT scanner is the detection principle used as explained before. A SPECT scanner uses only

information from single events, while the PET scanner detects coincidences that arise from the annihilation of the β^+ emitter explained before. This difference in the detection allowed the PET scanners to be used without collimators due to their lack of need to collimate the scattering photons, since these ones would not be counted as coincidences.

This difference allows the scanner to present some advantages against other types of diagnostic imaging, like the higher sensitivity (10^{-12} mol/L) or the quantifiability, since the signal obtained is proportional to the accumulated dose in the part of the patient being imaged.

Nowadays scanners have a full ring of detectors with the ability to detect these coincident high-energy gamma rays that emerge from the body in opposite directions (Figure 3). When two photons are recorded simultaneously by a pair of detectors, the annihilation event that gave rise to them must have occurred somewhere along the line connecting the detectors. Of course, if one of the photons is scattered, then the line of coincidence will be incorrect (Figure 5). After 100,000 or more annihilation events are detected, the distribution of the positron-emitting tracer is calculated by tomographic reconstruction procedures. PET reconstructs a two-dimensional (2D) image from the one-dimensional projections seen at different angles. Three-dimensional (3D) reconstructions also can be done using 2D projections from multiple angles. Nowadays all the scanners use the 3D technology. [8][9]

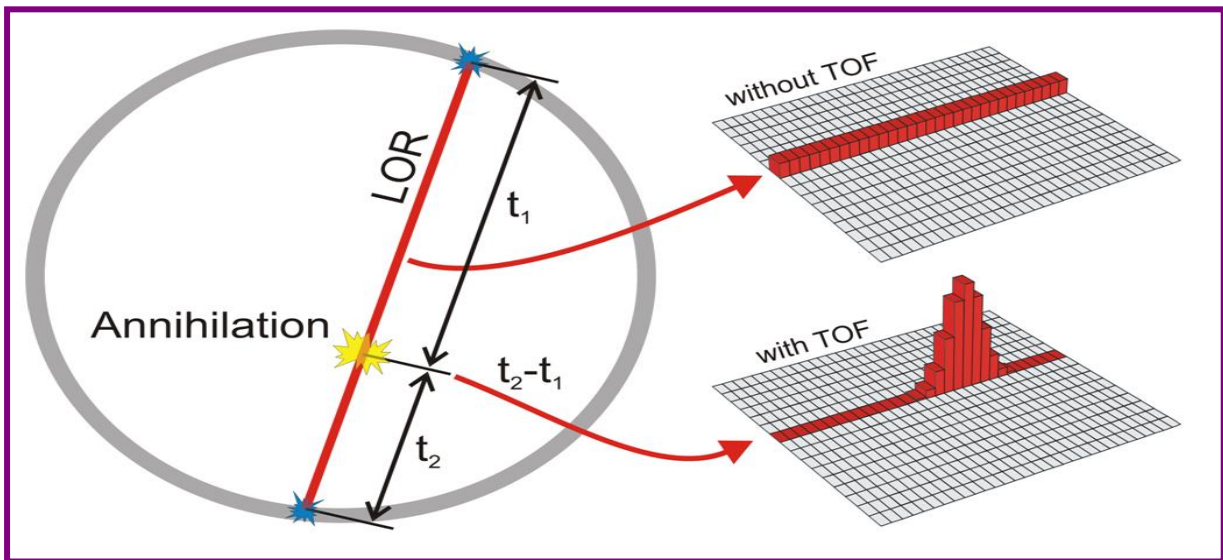


Figure 3: Schematic explaining the differences in the acquisition using Time of Flight and a regular PET scanner. [28]

The main difference between TOF PET and conventional PET is in the use of the line of response. The approach that is used almost universally involves the concept of computed tomography. By measuring the total radioactivity along multiple LOR in different angles through the object, mathematical algorithms are used to compute cross-sectional images that

reflect the concentration of the radionuclide in tissues throughout the body. By acquiring several of these lines it is possible to know where the annihilation is taking place.

The concept of time of flight is conceptually easier to understand, even though it is hard to use due to some equipment restrictions. This concept involves measuring the difference in arrival time of the two photons at the detectors. If an annihilation occurs closer to detector 1 than detector 2, then the annihilation photon directed towards detector 1 will arrive at that detector earlier than the annihilation photon directed towards detector 2. The relationship between the difference in arrival time of the two annihilation photons, Δt , and the location x of the annihilation with respect to a point exactly half-way between the two detectors, is given by

$$\Delta x = \frac{c(t_1 - t_2)}{2}$$

Where c is the speed of light (30cm/ns). The $t_1 - t_2$ (Δt) factor is the time difference used to extract the TOF information. The uncertainty in this measurement of time difference is called Coincidence Resolving Time (CRT) and is the main parameter used to define the quality of a TOF scanner. The parameter Δx is the spatial uncertainty that arises from TOF information. In order to achieve a Δx of 2mm we should have a 10ps CRT, which is not possible nowadays. With the current materials used in the detectors we have a spatial resolution of around 7.5cm, which comes from a CRT = 500ps. Because of the better noise performance of this technique, Time of Flight is incorporated in the tomographic reconstruction algorithm, contributing to the process of estimation of the radioactivity that best generates the measured projection data. This information, given by TOF helps to make the scanner less ill-conditioned. In non-TOF systems small errors in the input data can cause large errors in the final image. In TOF systems, the TOF information acts like a low-pass filtering making the system more resilient to artifacts, incorrect calibration/normalization. TOF is also decisive in reducing the signal to noise ratio (SNR). This reduction is more significant for large patients due to its relation with the diameter of the patient. The relation between the SNR of TOF and non TOF is explained in the following equation: [10]

$$SNR_{TOF} = \sqrt{\frac{D}{\Delta x}} \times SNR_{non-TOF}$$

This SNR improvement can be classified as a gain in SNR. It also known that TOF allows the reduction of the dose needed in a scanner since it acts as a sensitivity amplifier. This characteristic arises from the fact that the SNR is also proportional to the noise effective

counts (NEC), which results in better noise properties, giving an image that would have been obtained from an effectively higher number of counts without. Another advantage that comes from the previous characteristic is the reduction in the scan times of each patient, since it will be faster to achieve the desired image quality..[10]

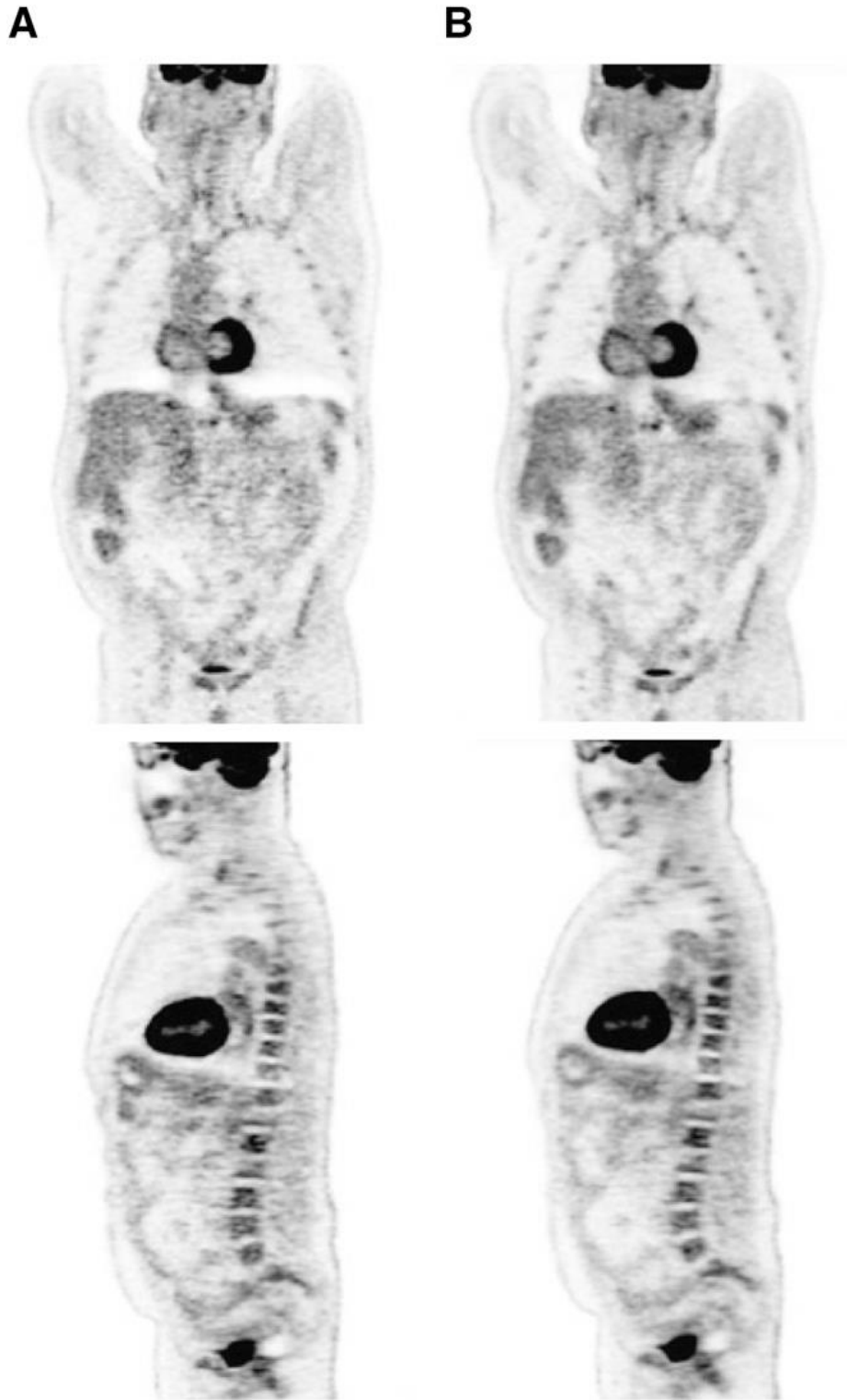


Figure 4: Example of the image that is possible to get in a PET scanner. On the left is the image of a common scanner and on the right is the image of a TOF scanner. On that image it is possible to observe the lower noise level. [29]

The image quality in a PET scanner is also defined by some other parameters besides the ones mentioned before. One of them is the type of events that can be detected in the ring of detectors. There are four different types of events that can be detected in a coincidence window (± 3 ns). These events are explained in Figure 5. The main objective in PET is to reduce to the minimum all the events that are not Trues.

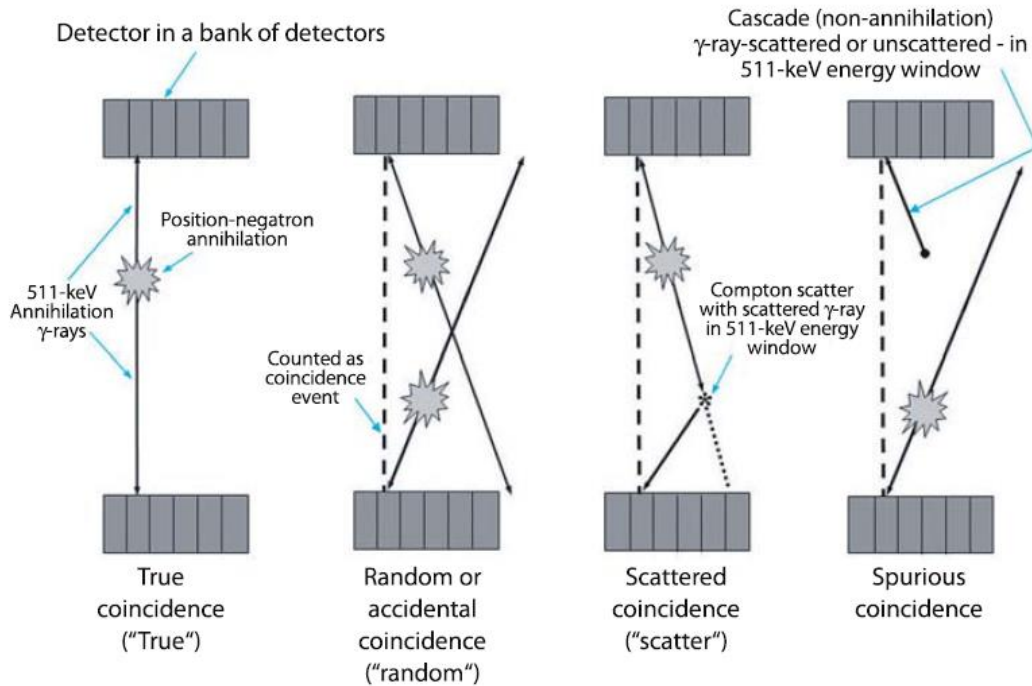


Figure 5: The four types of events that can be detected in a PET scanner. True events corresponding to the true detection of both photons that arise from the same annihilation and don't suffer any kind of scattering. Randoms which is the detection of two photons that come from different annihilations but are detected in the same LOR. There is also the scattering coincidence which can give rise to a false line of response. The last type of even that can be detected is the spurious coincidence which is another false coincidence originated by a random photon from another part of the body. [30]

Some of these scattered events can be rejected using a scintillator with high energy resolution and a short energy acceptance window, since it is expected that every photon that suffers some scattering carries a lower energy than an unscattered one. This is also an important factor in the search for the scintillators for the TOF PET, since the main goal is that they are fast, but they should also have an energy resolution (dE/E) as good as possible. The energy resolution of a scanner is measured through the FWHM function of the photopeak of the signal of photons with deposited energies of 511 keV. The state of the art scintillator that is available and presents the best energy resolution nowadays is LaBr_3 with an

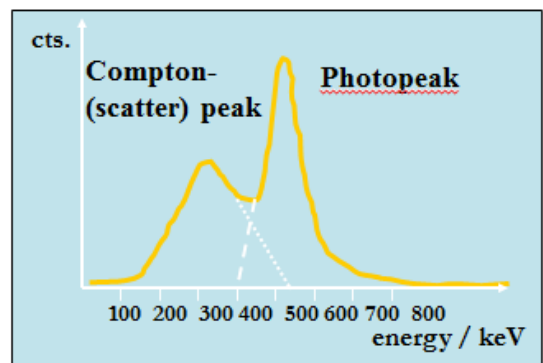


Figure 6: Example of the shape of the signal obtained in a detector.

energy resolution of 2.6%, but it is still facing some problems to be commercially used, since it is highly hygroscopic, shows intrinsic radioactivity (like LYSO) and the crystal growth mass production is still challenging. This has lead that LSO:Ce and LYSO:Ce crystals, with a better mass production characteristics (like yield), density (7.1-7.4 gcm³), high light yield with a short decay time compatible with TOF measurements. The most advanced PET scanners in the Philips portfolio (Ingenuity PET/CT, Gemini TF, Select TF) use the LYSO crystal with an energy resolution of ~11% (Figure 7) and a CRT time resolution of 480-590 ps FWHM. [11][12]. Similar solutions from Siemens and GE (besides the academia) also used the LSO/LYSO crystal scintillator family due to these characteristics.



Figure 7: Example of a Philips Gemini, a PET CT scanner commercialized nowadays by Philips. [31]

3. SCINTILLATORS FOR PET AND SPECT

Light detection is a powerful tool widely used nowadays in a lot of areas, including medicine. This is also the basic tool of Nuclear Medicine, since the scanners used convert the radiation into light which will generate an electric signal that will, ultimately, be converted into an image using reconstruction software. The process that includes the conversion of radiation until the generation of the electric signal is done in the detector of the equipment in nuclear medicine. This detector is one of the main components of the scanner as it can determine the whole quality of it.

The detectors used in PET nowadays are made with two major components: a photomultiplier tube (PMT) and a Scintillator crystal, which in case of Philips PET equipment is the LYSO crystal ($\text{Lu}_{1.8}\text{Y}_{0.2}\text{SiO}_5(\text{Ce})$).

A PET or SPECT detector consists of a set of a scintillator and Light detector that can either be a photomultiplier tube (PMT), like the ones used nowadays (Figure 8), or it can be an analog or digital silicon photomultiplier (SiPM, d-SiPM).

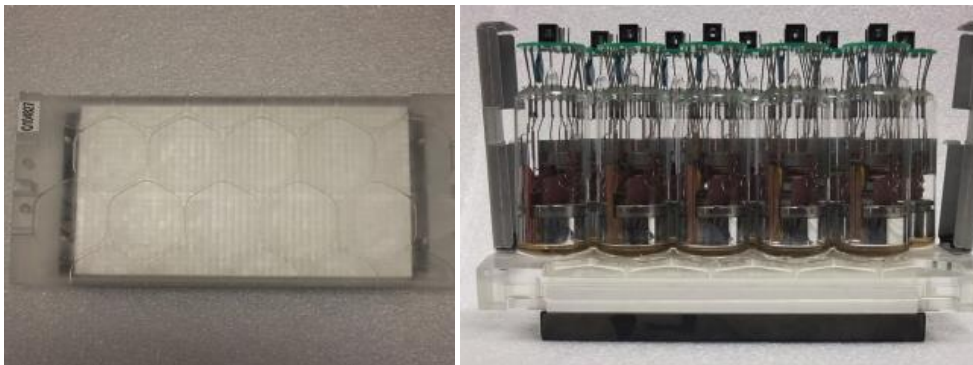


Figure 8: Example of a state of the arte PET detector used in the Gemini TF system. In each module LYSO crystals are glued to a light guide and readout by a set of PMTs. The module offers a CRT time resolution of 480 ps (new generation) up to 590 ps (second generation). [32]

3.1. Inorganic Scintillators in Medical Imaging

The scintillation process is one of the most useful methods to detect radiation. An ideal scintillation material should have a balance between the following characteristics:

1. High photopeak efficiency to get as many counts as possible;
2. High photon gain to have noise free signal with good energy resolution;
3. Linear conversion: the light yield should be proportional to the energy of the detected particles;

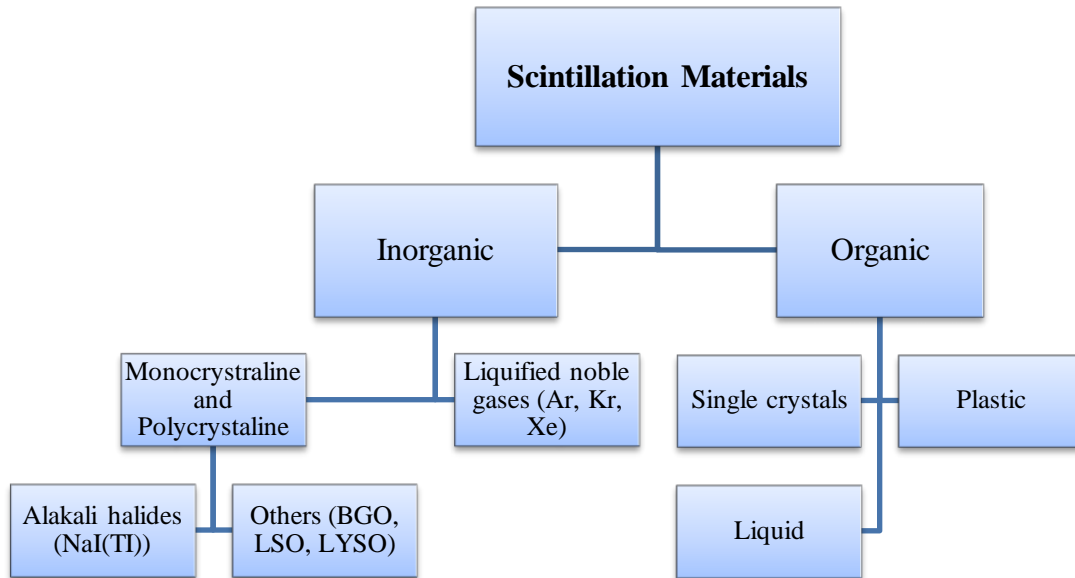


Figure 9: Schematic of the type of scintillators available.

4. The material should be transparent to its own wavelength emission, giving a light output as high as possible;
5. The decay time of the induced luminescence should be as fast as possible;
6. The material used should present a good optical quality and should be easy to manufacture;
7. The refraction index should be as close as possible to glass, in order to allow an efficient coupling to the light sensor.

Scintillators can be divided in two large groups: organic and inorganic, being the inorganic ones the mostly used in nuclear medicine. The inorganic scintillators usually have a higher Light Output (light generated per γ -ray absorbed) than the inorganics, even though they are also slower. Another advantage of the inorganic scintillators is their higher density (ρ) and their higher atomic number Z . This is an advantage since the absorption efficiency by photoelectric effect increases per $\text{cm} \propto \rho Z_{eff}^{3-4}$. Other of the advantages of inorganic scintillators is their easier reproducibility and large crystal growth. All of these characteristics together make them very suitable for the use in nuclear medicine. The organic scintillators can be used for fast electron detection or beta spectroscopy.[13][14]

Before explaining the full process by which a scintillator emits light it is important to distinguish between some different processes that lead to the emission of light. There are three main processes for light emission: fluorescence, phosphorescence and delayed fluorescence. Fluorescence is the process that leads to the prompt emission of visible radiation following some excitation. Phosphorescence is a similar process but this emission is slower and occurs at longer wavelengths. Delayed fluorescence has the same emission spectrum as the prompt

fluorescence but with an emission much later than the excitation. This delayed fluorescence is also known as afterglow. When looking for a good scintillator it is desired that most of the radiation is emitted as prompted fluorescence minimizing as much as possible the afterglow of the sample. [13]

The whole scintillation process can be divided in three main phases: conversion, transport and Luminescence. The conversion phase starts with the absorption of a high-energy photon by Compton or photoelectric effect. The latter will create an inner shell hole and an energetic primary electron, followed by a radiative decay (secondary X-rays), nonradiative decay (Auger processes and secondary electrons), and inelastic electron-electron scattering. [15]

The scintillation mechanism present in solid state inorganic scintillators is complex, because it includes: relaxation of the initial electronic excitation, thermalization and trapping of electrons and holes and possibly the excitation of the luminescence center. These processes happen due to the electronic band structure found in scintillation crystals. In the organic scintillators that can present luminescence due to their own molecular characteristics. The electronic band structure of a scintillator is similar to the one presented by semiconductors, where we

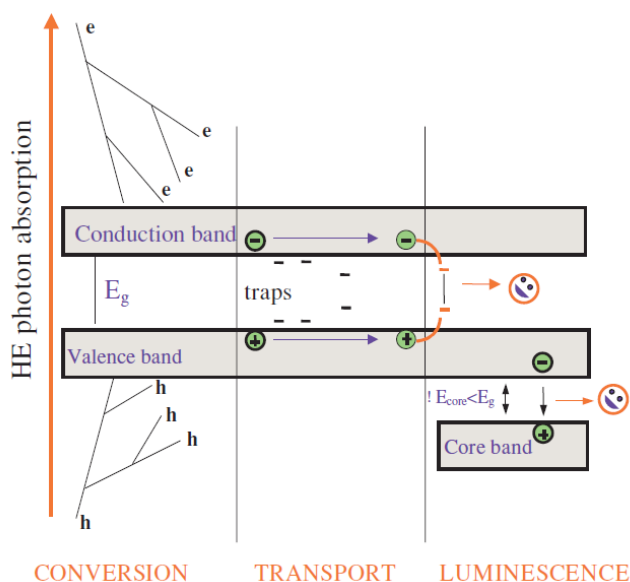


Figure 10: Schematic of the production of light in a scintillator [14]

have a conduction band, a valence band and an energy gap between both of them (Figure 10). The lower band is the valence band and it represents the electrons that are bound to the lattice sites. The conduction band represents the electrons that have enough energy to be free and migrate through the crystal. The band gap represents the range of energies in which we can't find electrons. In a pure crystal the absorption of energy in the scintillator can lift up electrons from the valence band to the conduction band, which creates holes in the valence band. Later in the process the electron that left the valence band can return there with the emission of a photon. But this process per se is inefficient. This inefficiency is due to the wide band gap which, if it is big enough, would create far UV luminescence instead of visible light. To

overcome this problem there are some impurities, also known as activators or dopants, that can be added to the crystal. The dopers create some special sites in the crystal lattice, changing the band gap structure creating intermediate energy states through which the electron can de-excite back to the valence band. This process will consequentially increase the probability of generation of visible photons, easily detected, because the energy between the sites is smaller than the band gap. The de-excitation sites are known as luminescence centers or recombination centers. Their energy structure determines the emission spectrum of the scintillator. [13]

A particle passing through the scintillator will generate a great number of electron-hole pairs by promoting the elevation of the electrons from the valence layer to the conduction layer. The hole, which is positively charged, will migrate to the activation site and ionize it which has lower ionization energy than the typical ionization energy of the lattice structure. Simultaneously with this migration the electron that was promoted to the conduction band can travel freely through the entire conduction band, and it will do it until when it finds an ionized activator site, creating a neutral configuration with its own excited energy states (Figure 11). If the activator state formed is in an excited configuration with an allowed transition to the ground state, its de-excitation will occur quickly and with high probability of an emission of a visible photon if the activator material is properly chosen. Usually the travel time for the electron to find an excited activator site is much shorter than the half-life of the photon emission, which implies that all the electron-hole pairs are formed immediately, and will subsequently be de-excited. This de-excitation determines the decay time characteristic of scintillators. Some scintillators can present only one decay time, while others, like the garnets studied in this project can present up to three different time constants: a fast one between 40 and 150ns, an intermediate one that can reach a few hundreds of ns and a slower one with some microseconds.

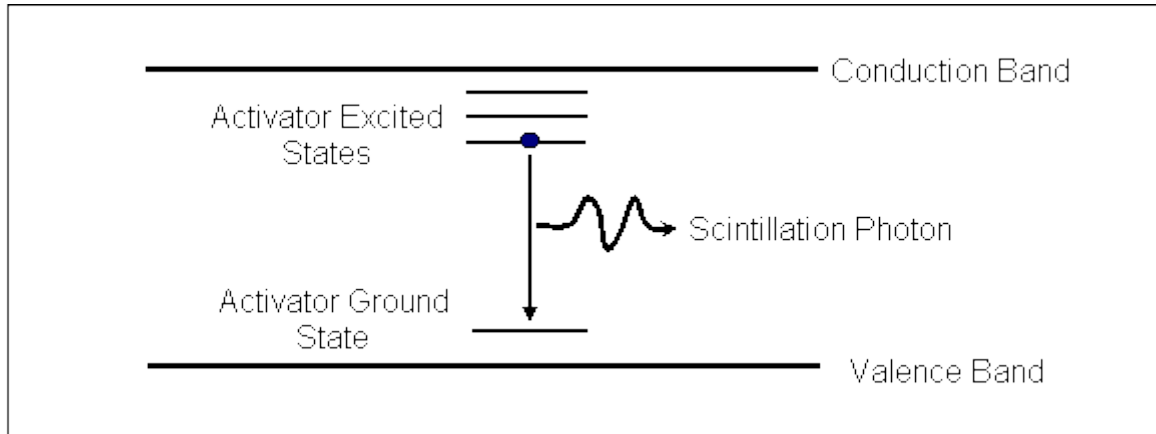


Figure 11: Energy band structure of an activated crystalline scintillator. [33]

It is also possible that the electron reaches an impurity site where it can't make the transition to the ground state. When this happens it is necessary to use more energy, usual thermal, to move the electron-hole pair to a level where the de-excitation is possible. Usually this is the process that generates phosphorescence, commonly called afterglow in scintillators.

There is another process that can happen in a scintillator, which is called quenching. This process happens when the de-excitation does not generate any visible photon, resulting only in some energy loss mechanisms in the conversion of the particle energy to scintillation light.

In all the processes mentioned above there is the possibility of the independent migration of the electron and the hole or, in alternative they can both travel together, in a configuration called exciton. This exciton can travel freely through the crystal until it reaches an activator site, where all the processes mentioned above can happen.[13]

Another reason to dope the pure crystals is to make them more transparent to their own light emission. Without the dopant, the energy required to excite an electron-hole pair would be the same liberated when the pair returns to the ground state. This would overlap the energy spectra of the emitted and absorbed radiation, making the crystal a self-absorptive. With the use of dopants the emission of light occurs at an activated site where the energy transition is less than that needed to create an electron-hole pair. This results in the emission at longer wavelengths decreasing the effect of the optical absorption of the bulk crystal.

Nowadays one of the most used dopants is Cerium (Ce). This dopant has decay time between 20 and 80 ns, depending on the host crystal, and usually presents a good light output, which puts Ce doped scintillators in an intermediate position between the organics and the older slow inorganic scintillators.

Besides the dopants, it is important to use the correct host material in a scintillator. The choice of a host material needs to fulfill the following requirements:

- a. Possibility to incorporate Ce^{3+} ions;
- b. Possess relatively small E_{gap} value;
- c. High density and a high Z.

Considering the above characteristics, nowadays the main hosts used belong to the silicates, oxides or garnets (used in this project), due to their crystal structure. As an activator one of the most used ones is the Ce^{3+} due to its high-efficiency emission of visible photons.

Even though Lu is not on the list of the best materials to incorporate in scintillator, it is used nowadays in Philips in the LYSO crystals due to its very strong photopeak absorption, increasing the stopping power of the crystal, giving the possibility to reduce its size. The main problems of using Lu in scintillators are its background radioactivity as well as its high price due to a low availability. [16]

To solve the problems of using Lu in scintillators a big part of scintillator research in last years has focused on finding new materials with similar characteristics that will allow the substitution of Lu. The criteria used to find new materials are exemplified in Figure 12. It was in this context that the idea of a garnet/ceramic showed up.

The figure shows a periodic table with the following annotations:

- Toxic:** Yellow background for elements like Li, Be, B, C, N, O, F, Cl, Br, I, At, Po, and U.
- Growth:** Green background for elements like Si, Ge, As, Se, and Te.
- Low E_{GAP} :** Orange background for elements like Ga, Ge, As, Se, and Te.
- Radioactive:** Red background for elements like K, Rb, Cs, Ba, La, Ce, Pr, Nd, Pm, Sm, Eu, Gd, Tb, Dy, Ho, Er, Tm, Yb, and Lu.
- Absorptive:** A label pointing to the transition metal region (d-block).
- No compounds:** A vertical label on the right side of the table.

Figure 12: Selection of the best elements for being the best host materials for gamma ray measurements based on the following criteria: toxicity, Energy gap, easy growth and intrinsic radioactivity. [11]

The main difference between a ceramic and a single crystal is in its microscopic structure. A single crystal contains only one single homogeneous structure. A ceramic is made of small crystalline structures. This difference is achieved using different methods for producing the scintillators. A ceramic is sintered from some previously mixed powders that are then put under very high temperatures for some hours, whereas a single crystal is grown in a complete different way. For instance for the LYSO crystal, used in Philips PET systems is

produced by the Czochralski method, since this method is suitable to grow single crystals. This method has the disadvantage of being more expensive than the ones used for growing ceramics like the ones used in this project. [17][18]

3.1.1. The LYSO scintillator

There are some characteristics that are useful to define if a scintillator is useful to use in PET or not, being the requirements needed for TOF PET different from the ones required for the conventional scanners that don't use TOF.

In Table 1 are some of these characteristics, and as an example we will use the LYSO crystal, since this is the scintillator used as reference in most measurements.

Table 1: Physical and Scintillation properties of some scintillators [12]

Scintillator	LYSO	BGO	CsI:TI
Density (g/cm³)	7.1	7.1	4.5
Light Yield (ph/MeV)	32000	9000	60000
Decay time (ns)	41	300	1000
Peak Emission (nm)	420	480	545
Energy Resolution (% @ 662 keV)	8	12	5
Hygroscopic	No	No	Yes

From the previous table it is possible to identify the characteristics that make the LYSO one of the best candidates for PET scanners. Comparing it with CsI:TI it is seen that it has a higher density and its much faster, even though it has a lower Light output that will reflect in a higher energy resolution. This factor is compensated with the possibility to use the TOF capabilities of the scanner, giving it a better quality. He higher density and also allows the decrease in the dose of radiotracers needed.

In the comparison with BGO (used by GE in some of their Discovery PET/CT systems) is also possible to see that the LYSO is not only much faster, but also with a higher Light output giving in the overall a much higher image quality.

The LYSO crystal has also the great advantage of his peak emission being close to the ideal photon detection efficiency of blue-enhanced PMTs as well as to analogue and digital SiPMs (dSi-PMs).

3.2.Photodetectors♦

In order to measure a signal from a scintillator it is necessary to use some photosensitive detector that is able to detect, amplify and convert the light produced by the scintillator. The main advantage of measuring light using these systems is the possibility to have a nondestructive analysis of a patient, the possibility to measure high-speed properties and a very high sensibility. These are all characteristics of a PET scanner.

The light detectors can be divided into three main categories, according to their operating principle: external photoelectric effect, internal photoelectric effect and thermal types. The external photoelectric effect works under the principle that when light strikes a metal or semiconductor in vacuum, electrons are emitted from this surface into the vacuum. This is the principle used in PMTs which gives them the best response speed and sensitivity, which is their ability to detect very low amounts of light, making them very suitable for use in medical equipment. The photodetectors that use the internal photoelectric effect can be divided into two types: photoconductive which uses photoconductive cells, and photovoltaic which uses photodiodes. Both types of sensors present a high sensitivity and minimum size compared to PMT. The last type of photodetectors, the thermal type, present a low sensitivity, but have the advantage of having no wavelength dependence, making them suitable for temperature sensors in fire alarms.[19]

In this chapter we will mainly focus on the PMTs and in the newly developed digital photomultipliers.

3.2.1. PMT

The most common type of photodetector used nowadays is the photomultiplier tube, commonly referred as PMT. A PMT is a vacuum tube with a glass window, a photocathode, focusing electrodes, an electron multiplier and an anode. All these components are sealed in an evacuated glass tube.

The detection and production of a signal in a PMT follows the following steps:

1. Light goes through the glass window;
2. Light will excite the photocathode which will allow the emission of photoelectrons into the vacuum via external photoelectric effect;
3. The released photoelectrons will be focused to hit the first dynode, where they will be multiplied through secondary electron. This process is repeated in each dynode, allowing an exponential increase in the photons number. The acceleration of the electrons between the dynodes is achieved through an electric field;

4. After the last dynode the electrons are collected by the anode.

Despite all the good characteristics of a PMT, these photodetectors have been losing some space to some more recently developed silicon photomultipliers (SiPM).

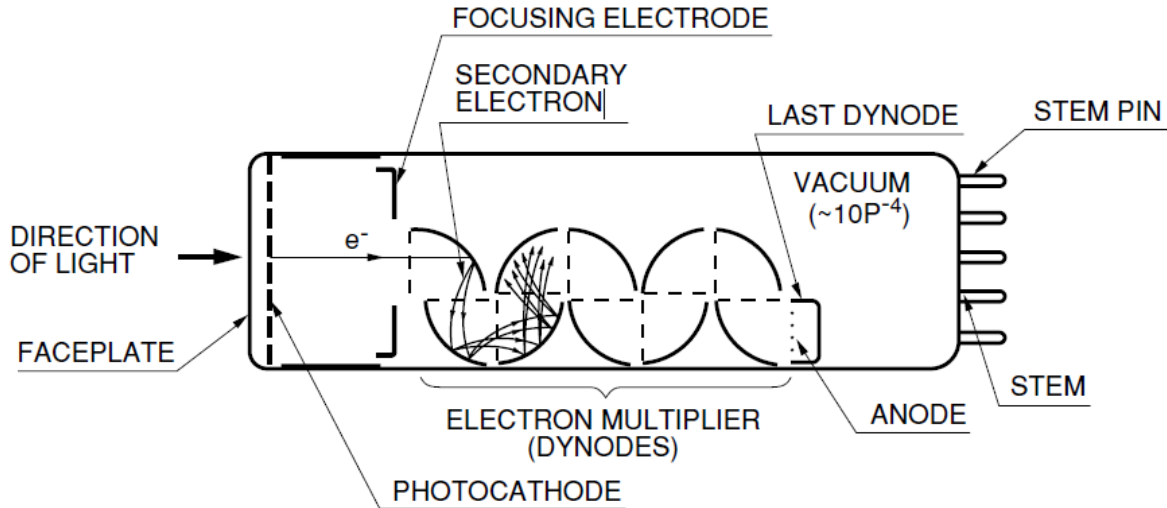


Figure 13: Components of a PMT. [19]

3.2.2. Digital Silicon Photomultipliers

SiPMs had recently gained interest as a replacement for PMTs due to their ruggedness, compactness and insensitivity to magnetic fields, which allows them to be used with an MRI in the newly developed Magnetic Molecular Resonance (MMR), which allows the simultaneous use of PET and MRI systems. As solid state detectors other advantage in the use of this type of scintillators is their low operating voltage, low power consumption and they are easy to fabricate. Anyway this type of photodetectors still present some disadvantages, like susceptibility to electronic noise, high sensitivity to temperature variations, and some limitations when detecting very low light signals.[20]

A SiPM can be made of arrays of avalanche photodiodes operated in Geiger-mode. This allows overcoming some of the problems in common solid state detectors, but still does not exploit the full capability of the Geiger-mode cells due to some parasitic inductances and capacitances that arise from the arrangement of electronics because a SiPM is made of passively-quenched cells, connected in parallel with a long interconnect that creates some of these problems. The resulting signal in a SiPM is therefore the analog sum of all the current in the cells.

Another problem of SiPMs is to read each signal when having thousands of channels. To overcome this problem a mixed-signal ASIC is needed to condition and digitize the SiPM

signal, but once again the addition of electronics to the set brings some more noise to the signal, especially because the detection of a single photon generates a signal of a few mV. To surpass all of these problems Philips Digital Photon Counting (PDPC) has created in 2009 the fully digital silicon Photomultiplier (D-SiPM), which converts each photon detected in a digital signal as early as possible in each of the Geiger-mode cells. In addition to this conversion, a complete trigger logic and a time-to-digital converter were integrated into the sensor. [20], [21]

Sensor architecture and characteristics

The PDPC D-SiPM plays a significant role in an acquisition, since it's by controlling the sensor that we can control some of the parameters of the acquisition, like the trigger level and validation thresholds. This is possible due to the ability of the detector to count single photons, as well as the presence of a time-to-digital converter (TDC). In all process the Scintillators described before just plays a passive role, giving the signal that will be read in photodetector.



Figure 14: Example of Philips D-SiPM [23]

The D-SiPM chip is made with 16 dies; each one of those will be connected to a crystal. Each die can then be divided in 4 pixels which give the photon count values (four photon counters per die). The pixels are in turn divided in 4 sub-pixels which are used to build the different trigger schemes used. These sub-pixels are then divided in smaller cells. Each die has 4x3200 cells.

The previous division allowed the simplification of the trigger levels. These trigger levels are used to determine when a signal is considered valid. In these detectors a trigger level is defined with the number of photons to consider it valid, and since these trigger levels are implemented at sub-pixel level they are applied using simple logic. There are four trigger levels which are summarized in Table 2. These trigger levels are defined before any acquisition. The importance of these trigger levels has to do with three factors:

- Time resolution: the smaller trigger threshold allows triggering on the first photon trigger yielding the best time resolution. Other trigger settings, trigger in higher number of detected photons. (Table 1). Since the detection process is stochastic additional time uncertainty is introduced at the higher trigger thresholds.

- Control of the dead time, which is the time after each event during which the die (set of 2x2 channels) can't record another new event. The higher the trigger level, the smaller the dead time.
- Reduce the importance of dark counts, defined as thermally generated carrier that can also start the avalanche process and be counted as true events. Dark counts can also be referred as noise.

The tiles used in this project allow the possibility to make a dark count map of the tile, and then switch off the cells with the highest dark count rate, bringing a bigger reliability to the measurements made.

Table 2: Resume of the logic involved in the trigger levels of the Philips D-SiPM sensor, as well as the average number of photons necessary to activate each trigger level. In the table sp1, 2, 3 or 4 stand for each sub-pixel in the die. [22]

Trigger level	Logic connection	Avg #photons to trigger
1	$Sp1 \vee sp2 \vee sp3 \vee sp4 \wedge$	1
2	$[(Sp1 \vee sp2)] \wedge (sp3 \vee sp4)$ \vee $[(Sp1 \vee sp4)] \wedge (sp2 \vee sp3)$	2.333
3	$(Sp1 \vee sp2) \wedge (sp3 \vee sp4)$	3
4	$Sp1 \wedge sp2 \wedge sp3 \wedge sp4$	8.33

On Figure 15 It is represented the acquisition sequence done with these tiles. In the beginning every electronic component is ready to start the measurement. As soon as the measurement starts, the trigger level, previously defined is activated, making the tile changing to a validate state. In this validation state the tile holds a previously settled time (5-40 ns) to achieve a minimum number of collected photons to make sure that the signal was not a dark counts. If the trigger (minimum number of photons collected) level is achieved, the acquisition starts. In this state, the pixel is activated while it waits for the scintillator pulse to completely decay. The signal here can be acquired between 5 ns and 20 μ s. The number of photons that reach the detector are stored while the detector doesn't reach the time for the acquisition. After this time the tile moves to the readout phase, where the number of photons detected in each line of the sensor is read and added to a photon counter. While one line is being read the previous one is recharged allowing a faster reset after the readout. After all this process each die becomes ready for a new acquisition.

One of the characteristics that all analogue or d-SiPMs show is the saturation that can occur when measuring the output of a scintillator with high light yield. This saturation is a

direct consequence of the limited number of cells present in each SiPM pixel. The saturation that occurs can be explained by:

$$k = N \cdot (1 - e^{-p/N})$$

Where k is the number of triggered cells, N is the total number of cells and p the number of photons that would have been detected. Using the previous equation the number of photons that should have been detected can be calculated using the following equation:[21]

$$p = -N \cdot \ln(1 - k/N)$$

This saturation behavior can interfere with the linear behavior of the SiPM. To correct for this, a saturation correction can be applied either during the data processing or in real-time by an on-board FPGA.

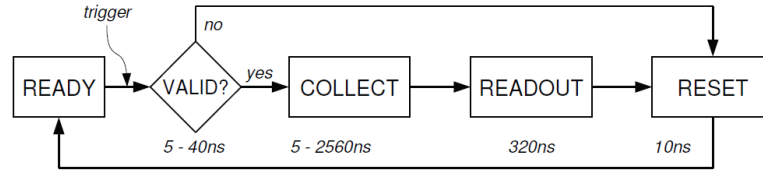


Figure 15: Schematic of the validation method that occurs in Philips d-SiPMs. [22]

Another problem faced by analogue SiPMs is the temperature dependence, since temperature affects the ionization coefficients of electrons and hole in the silicon. This leads to a change of the breakdown voltage according to temperature and a consequent change in the gain of the detector. The temperature dependence can be very significant in analogue SiPMs up to 2-4%/K depending on the vendor. The Philips DPC D-SiPM minimizes this by design, allowing minimizing the temperature dependence down to about 0.2%/K. Another parameter affected by temperature is the dark count rate, which increases with the increase in temperature.

Apart from all the parameters described above, another parameter very useful to define the behavior of an analogue or D-SiPM is the photon detection efficiency (PDE), which is the probability to detect a photon of a certain wavelength. This is an intrinsic property of the materials used in the construction of the detector. The detectors used in Philips are more sensitive in the blue area, having their wavelength peak sensitivity (λ_p) near the 420nm in order to match the emission spectra of LYSO:Ce (Figure 16).

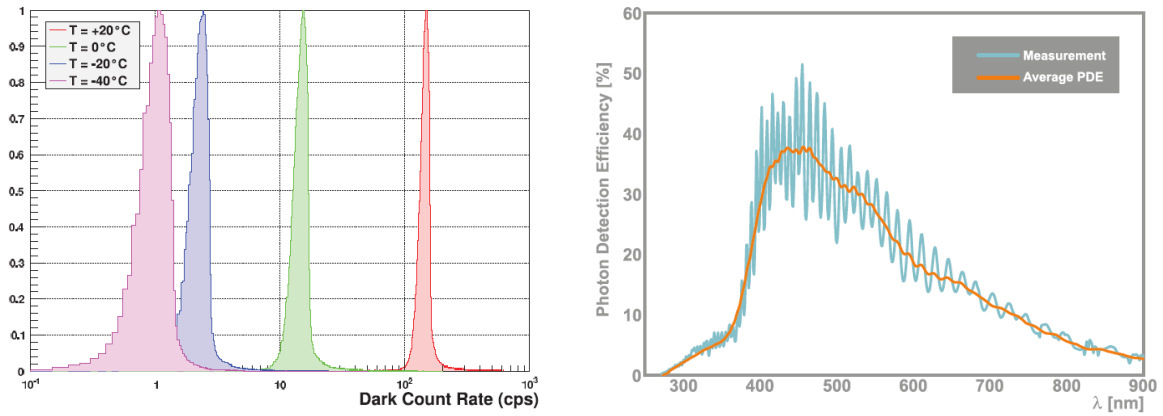


Figure 16: On the left Histogram of a dark count map at different temperatures. [21] On the right: a typical distribution of the PDE of Philips PDPC D-SiPM sensor. [23]

Table 3: General characteristic of the d.SiPM used in this project.[23]

Physical characteristics	DPC3200-22-44
Outer dimensions	32.6 x 32.6 mm ²
Pixel pitch (H x V)	4.0 mm x 4.0 mm
Pixel active area	3.9 x 3.2 mm ²
Number of cells per pixel	3200
cell size	59.4 x 64 μm ²
Spectral response Range	380 nm – 700nm
Peak sensitivity wavelength (λ_p)	420 nm
PDE @ λ_p (pixel level)	40%
Pixel fill factor	74%
Tile fill factor	75%
Dark count rate (95% cells active)	< 7MHz / pixel at room temperature
Operational bias voltage	27 +/- 0.5 V
Intrinsic timing resolution	44ps

4. EXPERIMENTAL METHODS

All the measurements here presented were made to test the ceramic garnet scintillators performance under conditions similar to the PET scanner, i.e. excite with 511 keV gamma radiation and measure in coincidence. The source of γ -radiation used in both experiments was a Na-22 source, because of its β^+ decay and consequent emission of two photons of 511keV necessary to detect coincidences.

4.1.PMT Measurements

The main goal of the PMT measurements was to perform the evaluation of the decay times of the samples available (powders, disks and sticks).

These measurements were made at room temperature using two PMTs mounted in a vertical position. On the window of the top PMT (PMT 1) was a LYSO crystal, which was used as a reference for all the measurements. On the window of the bottom PMT (PMT 2) was the sample that was being tested (garnet, disk or powder). Between both arrays was the radioactive source. These PMTs were both connected to HV supplies and to an oscilloscope that was used to collect the data and to set the right parameters for the measurements. Figure 17 shows schematically the experimental design used in the PMT measurements.

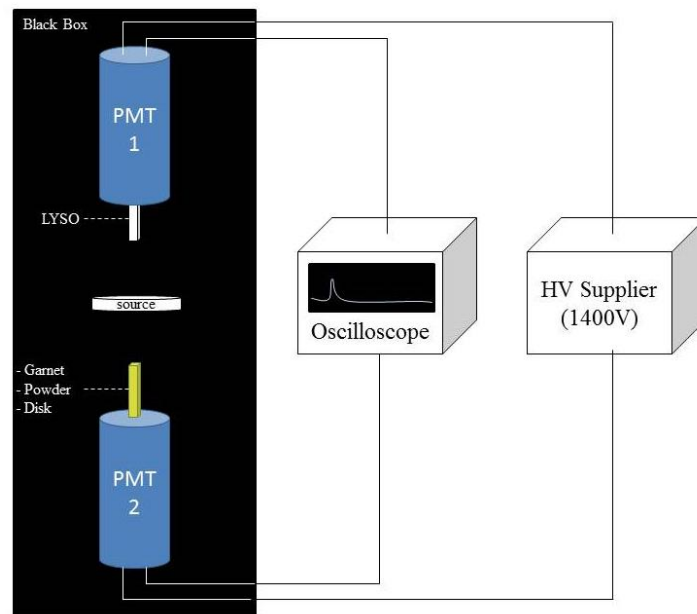


Figure 17: Schematic of the PMT measurements.

For the measurement, the garnets and the disks used were optically coupled to the PMT using a silicone paste. This paste was necessary to achieve a better light transmission

between the PMT and the sample. In the powder measurements this paste wasn't used. To achieve a higher signal a reflector was used in every measurement. For the sticks we used a case made of vikuity reflector sheets (Figure 18 left), for the powders we also used a layer of vikuity, but covering only the top of the powder. The disks had their own white reflector case. To measure the powders it was necessary to use small plastic containers, in the form of a disk which allowed the powder to be pressed, presenting a homogeneous powder layer (Figure 18 right).

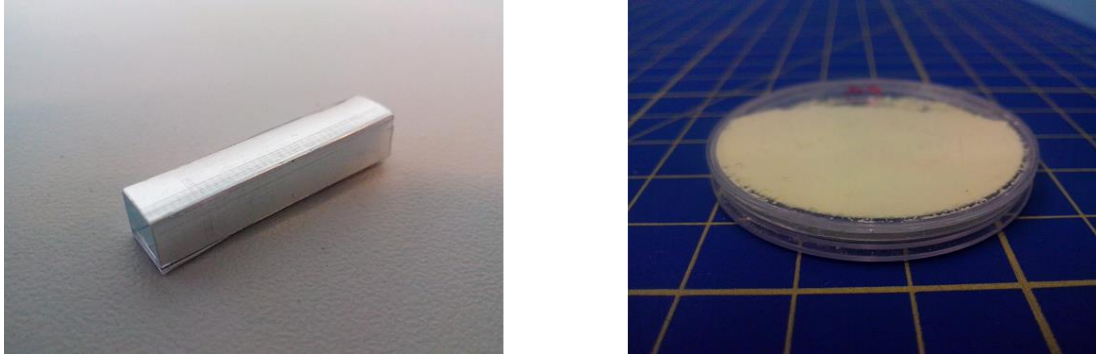


Figure 18: On the left, an example of the vikuity case used to measure the sticks. On the right: an example of the plastic disks containing the powders.

In order to only acquire data from coincidences and to suppress scattered radiation of lower energy, trigger levels were set in the oscilloscope. These levels were defined in terms of voltage. The channel from PMT1 was set to -50mV and the channel from PMT2 was set to -80mV. The value on PMT2 had to be adjusted sometimes because of the different signal height from different samples. For instance the trigger level used for powders was around -20mV because of their low signal. With these trigger levels an event was considered true, and consequently counted, if both PMTs achieved the required voltage level in a time window of 2ns. The overall signal was acquired for 10000 events (coincidences) with an integration time of 20 μ s. The data acquired from the oscilloscope was the data from the PMT2. A review of the settings used is listed on Table 4.

Table 4: Resume of the settings used in the PMT measurements.

Settings	Values
High Voltage	1400V
Current Intensity	0.72mA
Trigger PMT 1	-80 mV
Trigger PMT 2	-15 to -80 mV
Number of acquisitions	10000
Coincidence window	2 ns

In the PMT measurements, the first evaluation of decay times was made in powders. Because of low light output and high levels of scattering the trigger levels had to be adjusted to lower levels. The second evaluation was made on disks. After the evaluation in powders and disks, the best samples were selected to the next phase that consisted in building a batch of sticks that would be used in the TEK measurements described in section 4.2.

4.1.1. PMT measurements: Analysis

After the acquisition of the signals, an analysis was done in order to obtain the decay values. This analysis was the same for every sample, changing only some values in the Matlab script used.

All the measurements performed were evaluated using Matlab and Origin. The first step in this evaluation was to convert the file acquired from the oscilloscope to a matlab file. The second step of the process in Matlab followed three main steps:

1. The program determined the start of the signal using a single trace;
2. The single trace were used as a reference to rule out every of the 10000 traces that were somehow corrupted e.g. by a second gamma photon hitting the PMT during the readout time, or due to a low or high signal.
3. The final step was just to make the average of all the relevant traces.

The final step in the analysis was made with Origin. In Origin the objective was to read an ASCII table that resulted from the Matlab analysis and then perform several evaluations as: the integral within 645 ns and then the peak of the decay curve. These values were used to calculate the effective decay times of the samples. This effective decay time is calculated dividing the peak value by the integral over a defined period of time (the formula is explained in Chapter 6-Discussion). In this evaluation was also used a tool from origin to automatically calculate the decay times and the respective percentage that each decay time represented.

4.2. Philips PDPC TEK Measurements

Measurements using a Philips PDPC TEK unit (Technology Evaluation Kit) were made to assess the values for CRT, Energy Resolution, Count Rate and Light Output (LO) were obtained. The main differences between this measurement and the PMT measurements were:

- the type of detectors used: d-SPMs were used instead of a PMT;

- the ambience temperature: PMT measurements were made at room temperature and here a climate chamber was used;
- the number of crystals used: in the PMT the measurements were made on single crystals and here we used arrays of 64 crystal pixels.

The main reason for using the PDPC sensor instead of the PMT setup was in fact the possibility to readout up to 64 crystal pixels in one acquisition.

TEK measurements were made in a climate chamber in the dark at a temperature of 5°C. For these measurements two arrays were used. This allows to measure in coincidence. One of the arrays was used as a reference, composed of only LYSO crystals arranged in a matrix of 8x8 crystals. The second array was also built as well with 64 crystals with the central matrix of 4x4 crystals built with the garnets that were being studied as you can see in Figure 19. The remaining array was made with LYSO:Ce pixels.

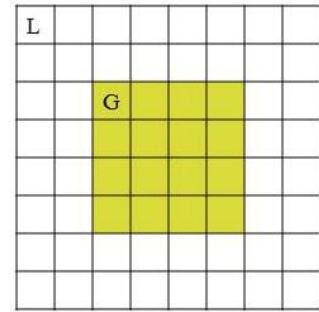


Figure 19: Schematic of the arrays used (top view). The white squares represent the LYSO crystals and the yellowish ones represent the garnets.

These TEK measurements were made using two different trigger levels: trigger 1 and trigger 2. The difference between these trigger levels was the number of photons needed to provide a valid signal. In trigger 1 only one photon was needed to make a valid signal. In trigger 2 this number was an average of 2.33 photons. This number is explained because the trigger needs to happen in two different sub-pixels, and there is a chance that the 2nd photon would hit the same sub-pixel. The signal was acquired for 500000 single events with a signal length of time of 20 μ s. In Table 5 there's a resume of the parameters used in the acquisitions.

After the measurements the data was analyzed in a specific Matlab script which allowed obtaining the number of coincidences registered as well as the CRT, LO, energy resolution and number of counts.

Table 5: Settings used for the TEK measurements.

Setting	Values
Integration length	325, 645 and 1245 ns
Signal length	20 μ s
Trigger level	1 and 2
Coincidence window	10 ns
Number of frames acquired	500000
Temperature	5°C

Both measurements were made following the safety instructions from the Philips Research Eindhoven Radiation Protection Officer, which included the use of a personal badge as well as an online course about managing radiation sources. Concerning the powders, because of their nature, it was necessary to use gloves and a mask for breathing.

4.2.1. Preparation of the array for TEK measurements

The preparation of new arrays involved the placement of the individual crystals in a reflector array, with spaces for 8x8 crystals. The inner central part of 4x4 crystals was filled with different versions of ceramic garnets, and the outer ring with LYSO:Ce crystals. The arrays were recycled which means that only the garnets that are being tested were changed, leaving the LYSO unchanged.

5. RESULTS

In this chapter I present the most relevant results achieved in the PMT and PDPC TEK measurements. In most results presented the comparison is made between the results of the ceramic garnets and the LYSO, which is the scintillator used nowadays. Results are also compared with GAGG:Ce crystal scintillator from Furukawa. This scintillator uses similar materials to the ones used for the ceramic garnets but they are grown as a standard crystal.

5.1. PMT results

The results obtained with the PMT measurements were mostly used to have an evaluation of the decay time (fitted using Originlab™ and the effective decay time, which arose from theory) of each sample used. These results were used to acquire information about the trends of decay time of garnets.

The first part of the PMT results are shown as an example of the signal measured in the PMT for various samples, including the ones used as a reference. All the signals were obtained under the same conditions.

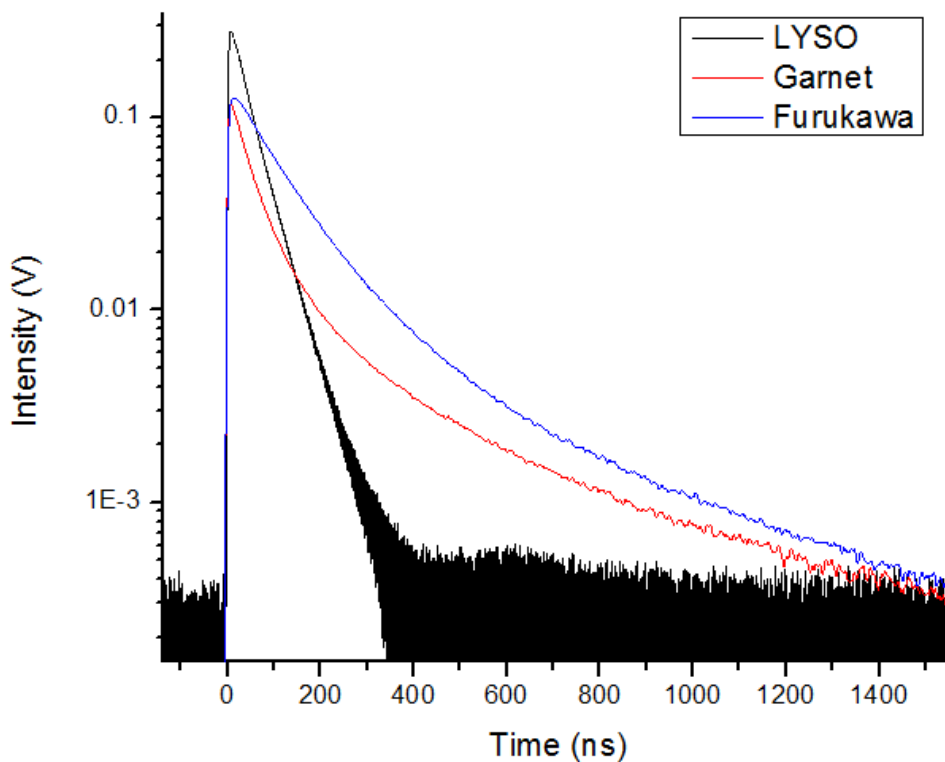


Figure 20: Comparison of the signal obtained from different scintillators: Garnet 165-3 (black), LYSO (red) and Furukawa (Blue).

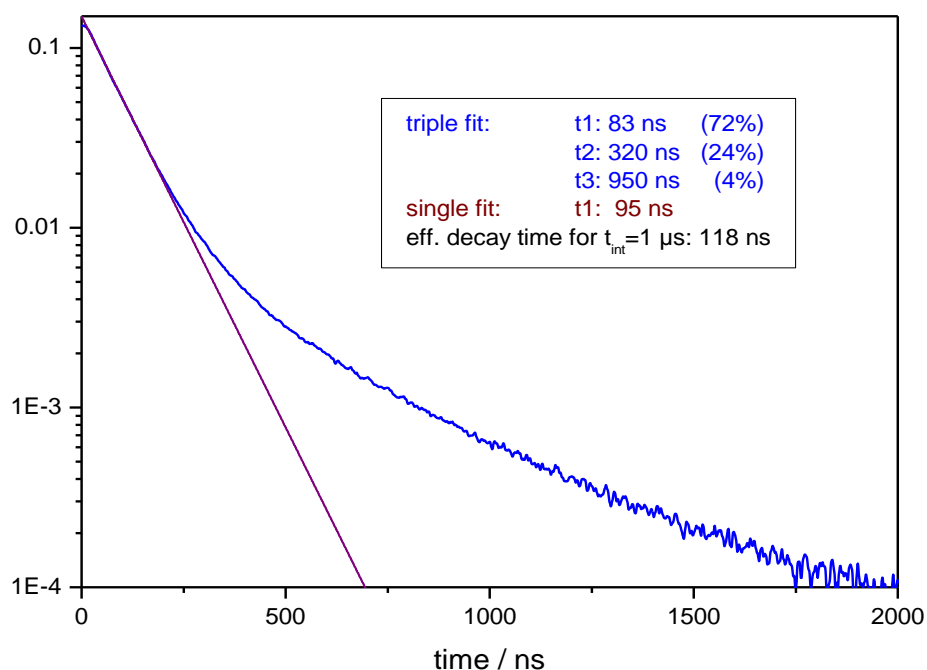


Figure 21: Graphic showing the effects of using different fits to get the values of the decay times. For comparison is also shown the value of the effective decay time for the same sample.

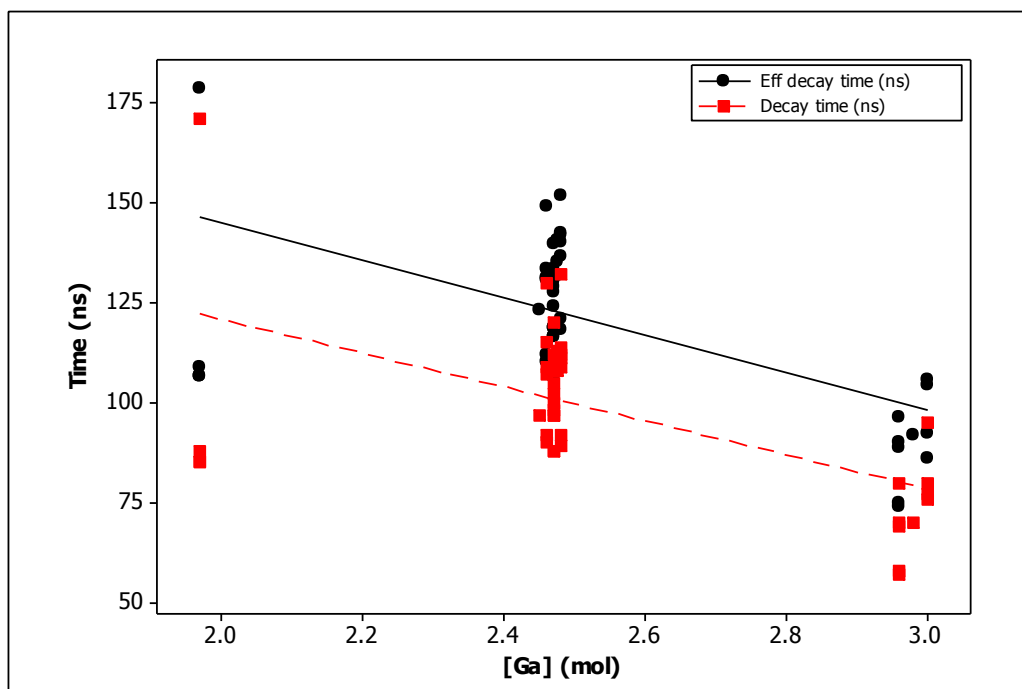


Figure 22: Trend of the effective decay time according to different concentration of cerium and gallium on sticks. Settings used in the acquisition: trigger 1 and 2 = -80mV; overall acquisition time = 20 μ s.

5.1.1. Results from powders:

In this chapter we will show the results gathered from the powders measured in the PMT setup. The powders allowed to obtain the first trends of results

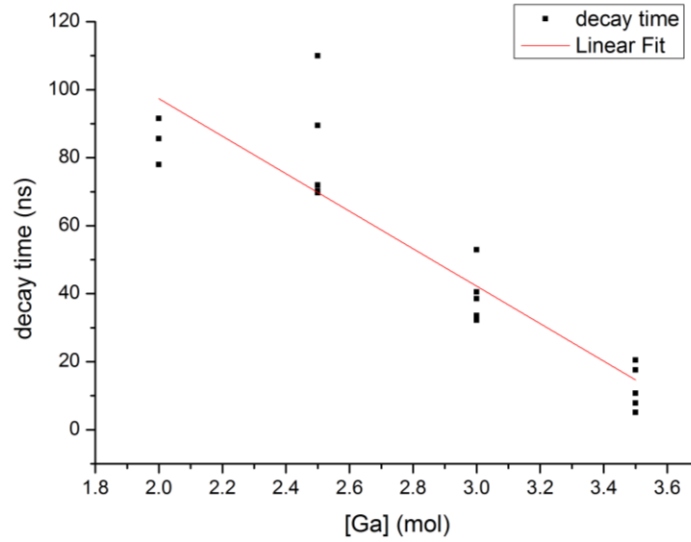


Figure 23: 2-D plot showing the effect of the Ga content in the decay time. The linear fit was used only as a figure to show the general trend.

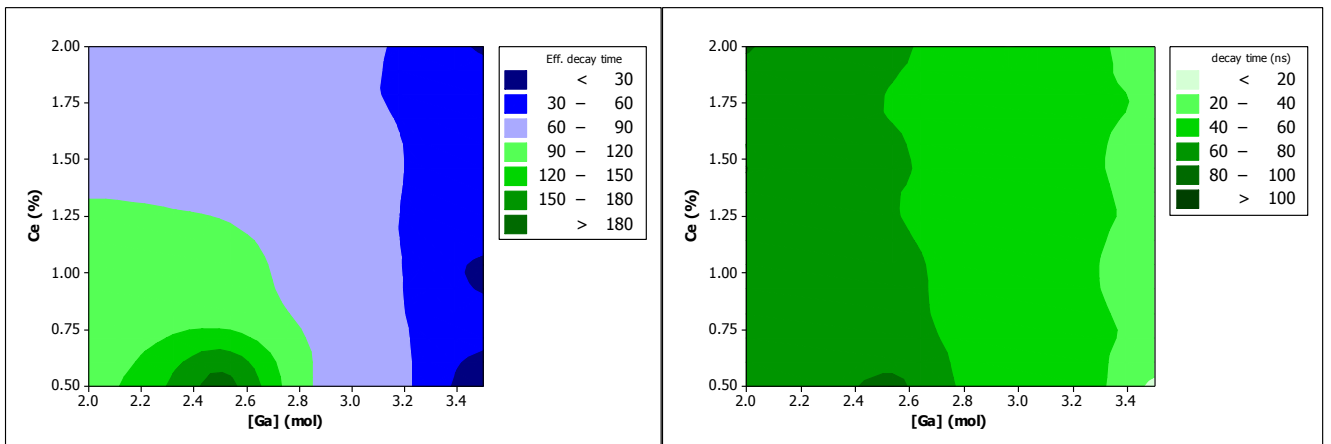


Figure 24: Graphics with the trends of decay time and effective decay time according to different concentration of Gallium and Cerium on powders.

Results from disks

Here will be presented the results that were obtained from disk samples. The trends will be shown for the effective and the decay time, even though the general trend is similar.

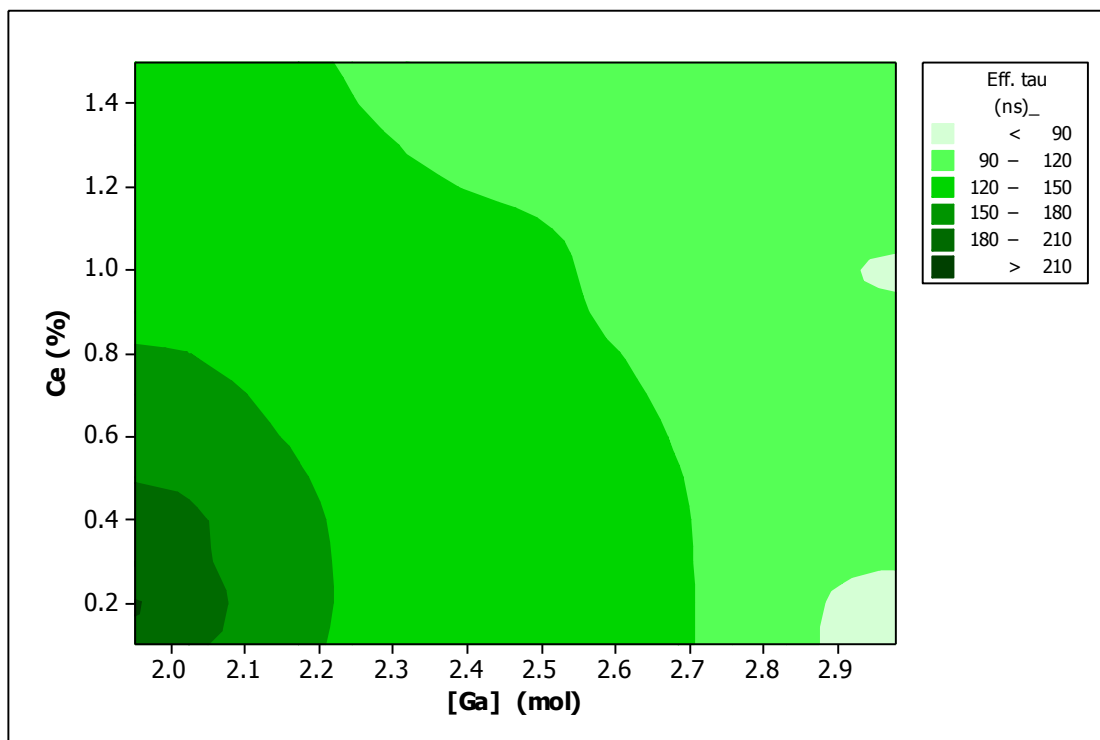


Figure 25: Trend of the effective decay time according to different concentration of cerium and gallium on disks. Settings used in the acquisition: trigger 1 and 2 = -80mV; overall acquisition time = 20 μ s.

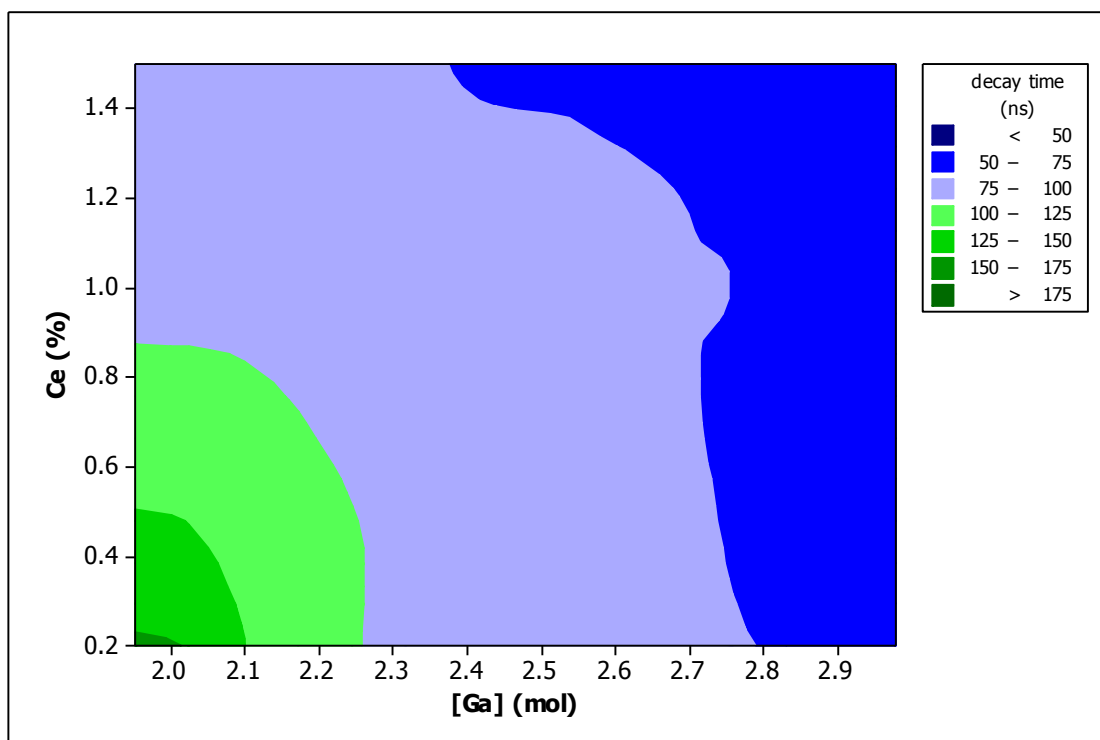


Figure 26: Trend of the decay time according to different concentration of cerium and gallium on disks. Settings used in the acquisition: trigger 1 and 2 = -80mV; overall acquisition time = 20 μ s.

Results from sticks

Here will be presented the graphic with an overview of the results gathered from the PMT measurements for sticks. The results are shown as a trend by the composition of the stick.

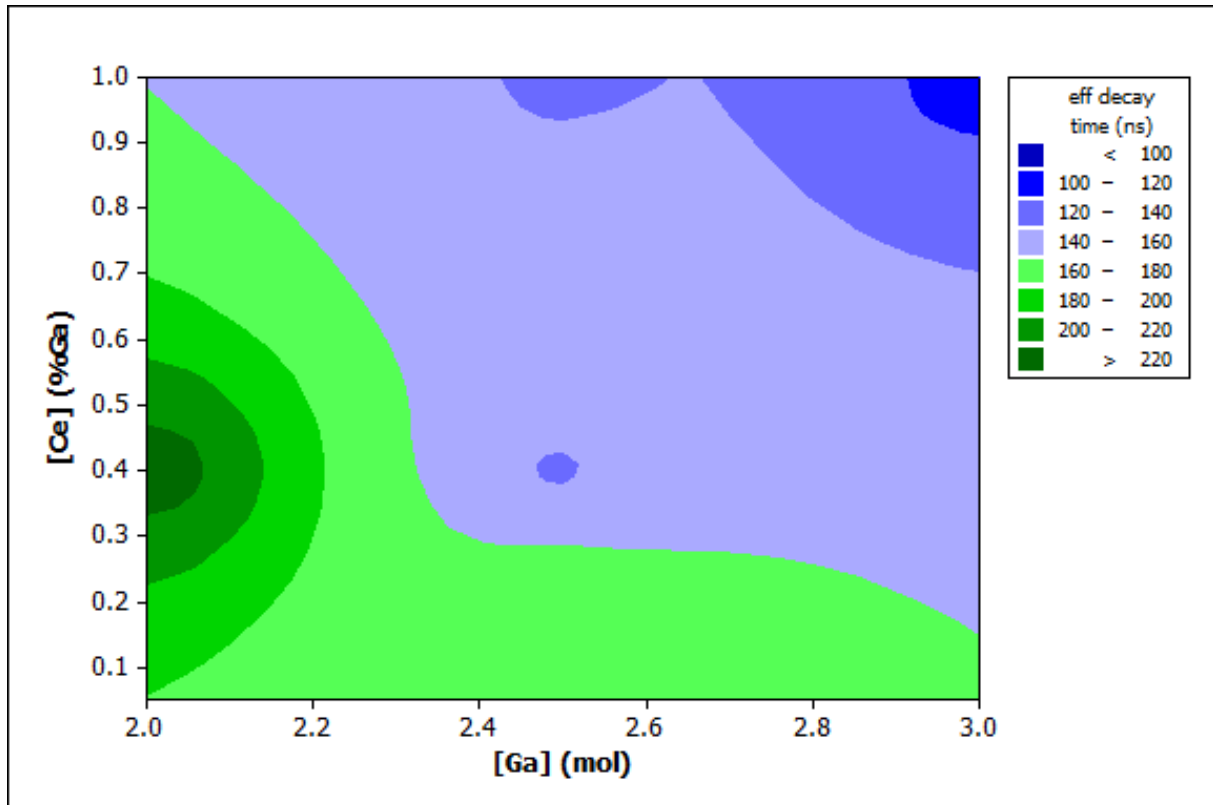


Figure 27: Trends showed by the PMT measurements on sticks.

5.2. TEK results

In Figure 28 examples of the results gathered from the Matlab script are shown. All of them were obtained for an integration time of 1280 ns with trigger 2, but the results acquired with trigger one were similar.

lyso	lyso	lyso	lyso
lyso	Garnet	Garnet	lyso
lyso	Furu	Garnet	lyso
lyso	lyso	lyso	lyso

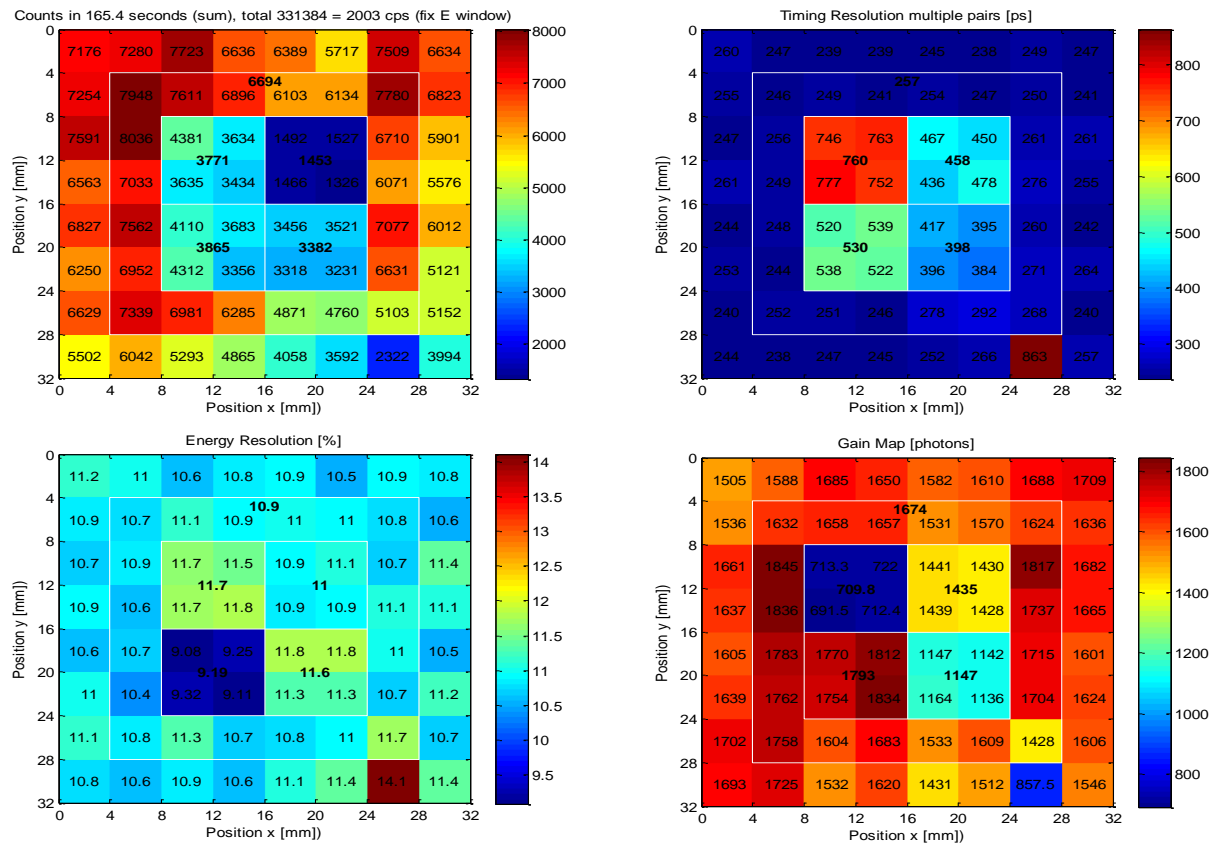


Figure 28: Example of the graphics obtained with Matlab for one of the arrays measured. The two outside layers are made with LYSO. The core is built with four different garnets, following the schematic presented before. From left to right, top to bottom there is: The counts, the CRT, the energy resolution and the number of photons. On top there is the schematic of the disposition of the crystals in the array.

Overview of TEK results:

Here I present four graphics with an overview of the results gathered from TEK, which include coincidence resolving time, Light Output, Energy Resolution and Counts against LYSO and GAGG:Ce Furukawa. The values shown are the average of all the measurements performed for all the samples.

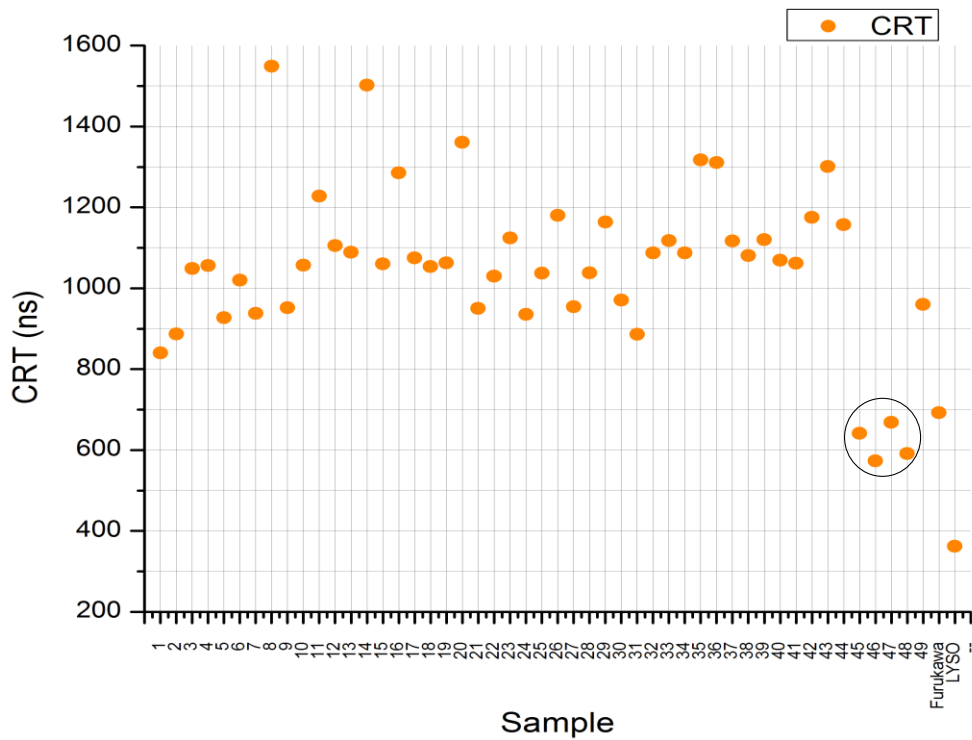


Figure 29: Overview of the CRT values of some of the samples measured. The lowest value achieved still belongs to LYSO, but some of the garnets were able to surpass the values of Furukawa. The four samples inside the circle are the ones that present better CRT values than the LYSO.

The values of CRT from our garnets vary from 1650ns to 590 ns. Four of the our ceramic garnets were faster than the Furukawa GAGG:Ce samples, which present a CRT value of 691 ns. The LYSO shows the best CRT of 362 ns.

In Figure 30 there an overview of the Light Output values of ceramic garnets compared to the LYSO and Furukawa is shown. The range of values from the garnets goes from 2000 to the lowest value located below 500 photons. Once again there were some samples that got better values than the ones from Furukawa (1681) or LYSO (1745).

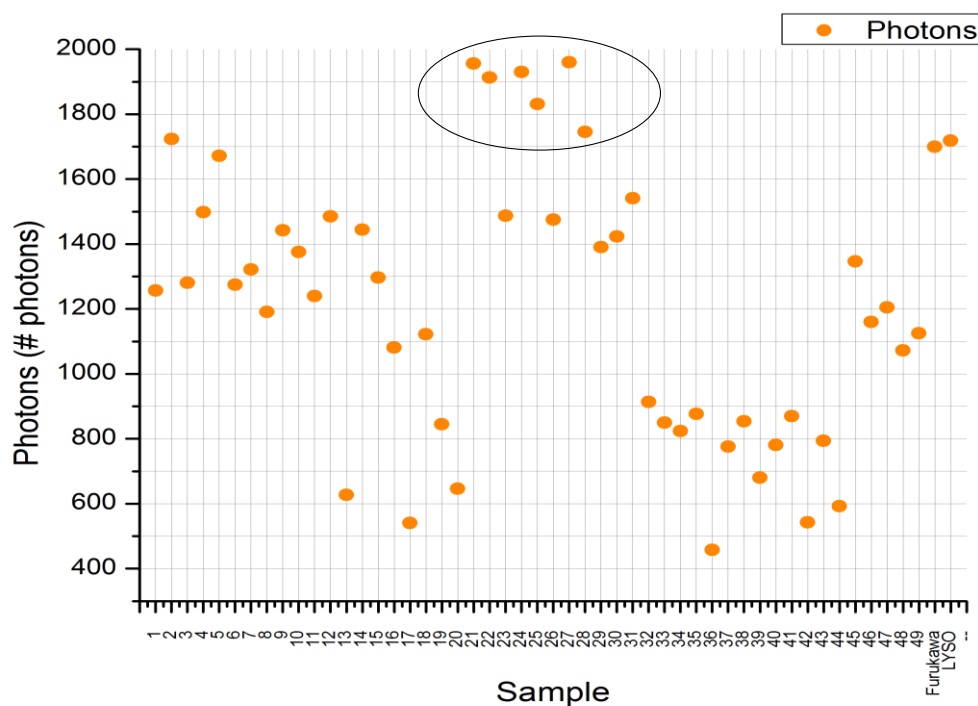


Figure 30: Overview of the LO values our gamets.

In Figure 31 the overview of the Energy resolution of the ceramic garnets is shown. The values gathered range between 8.43% from sample 13 until 17.1% in sample 43. The value from Furukawa is 9.45% and the value from LYSO is 10.8%.

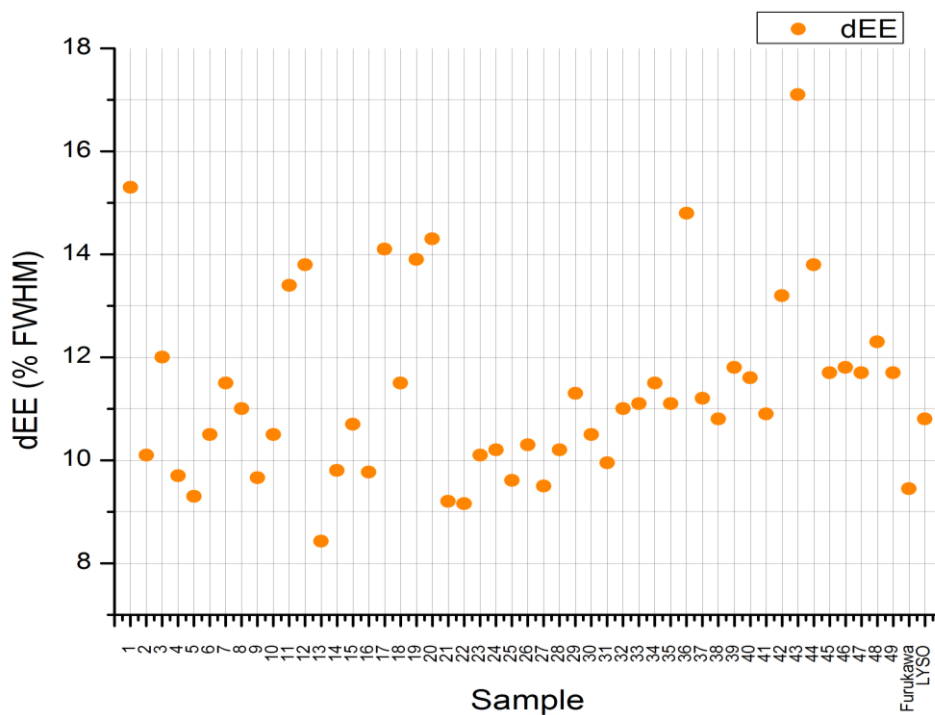


Figure 31: Overview of the dEE results.

To finish the overview in Figure 32 the number of counts normalized to LYSO is shown. The number of counts in LYSO is considerably higher than every other sample measured, even the GAGG:Ce Furukawa. This is due to the higher density and effective Z of

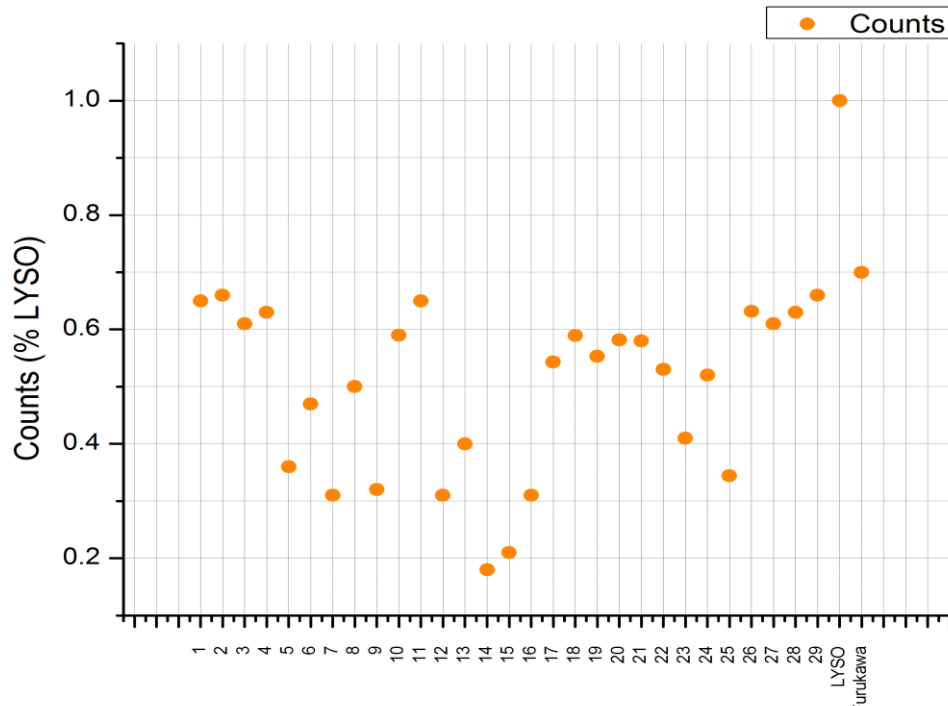


Figure 32: Overview of the number of counts normalized to the number of counts of the LYSO.

the LYSO in comparison with the ceramic garnets and GAGG:Ce

On Figure 34 is the graphic showing the general trend of the values of CRT with the change in the concentration of Gallium and Cerium.

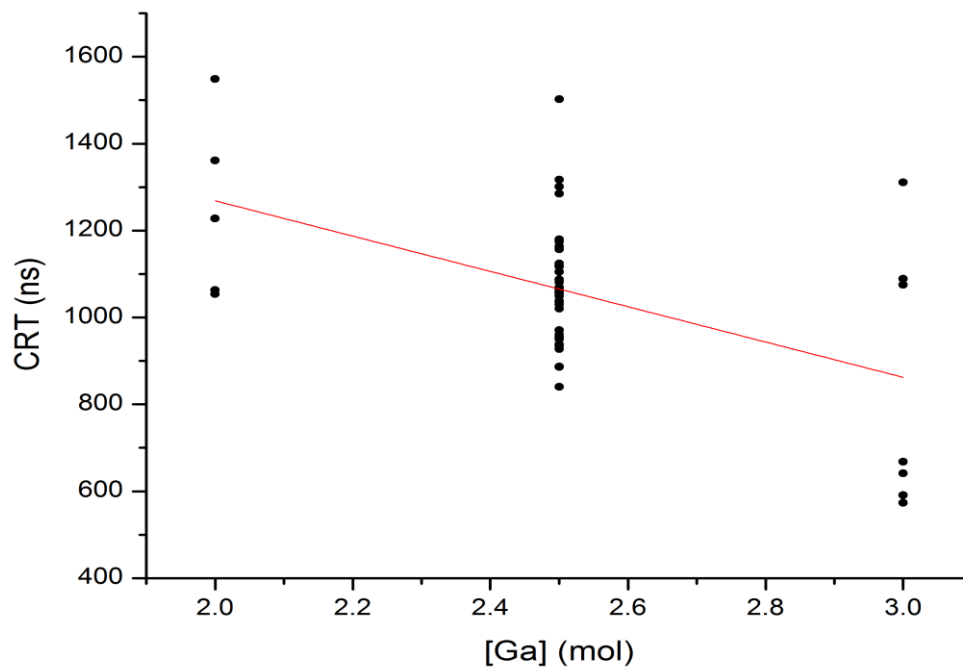


Figure 33: CRT behavior in garnets according to the concentration of Ga.

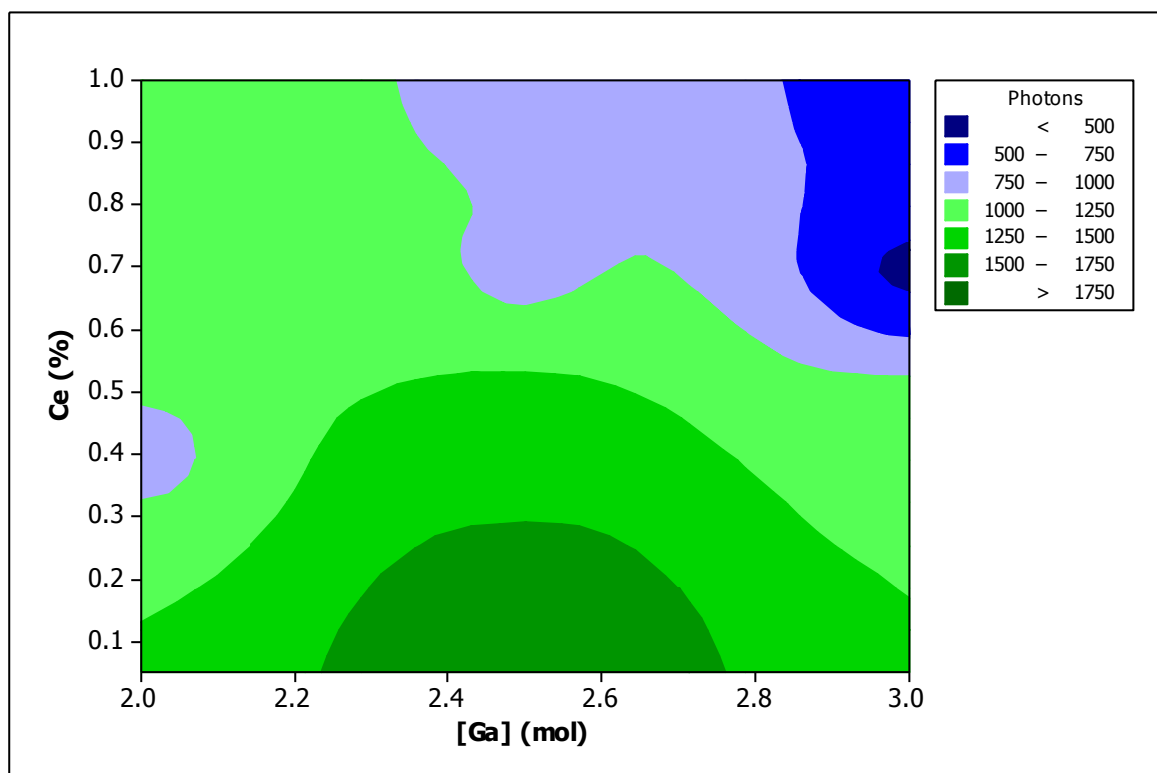


Figure 34: Trend of the LO with Ce and Ga content.

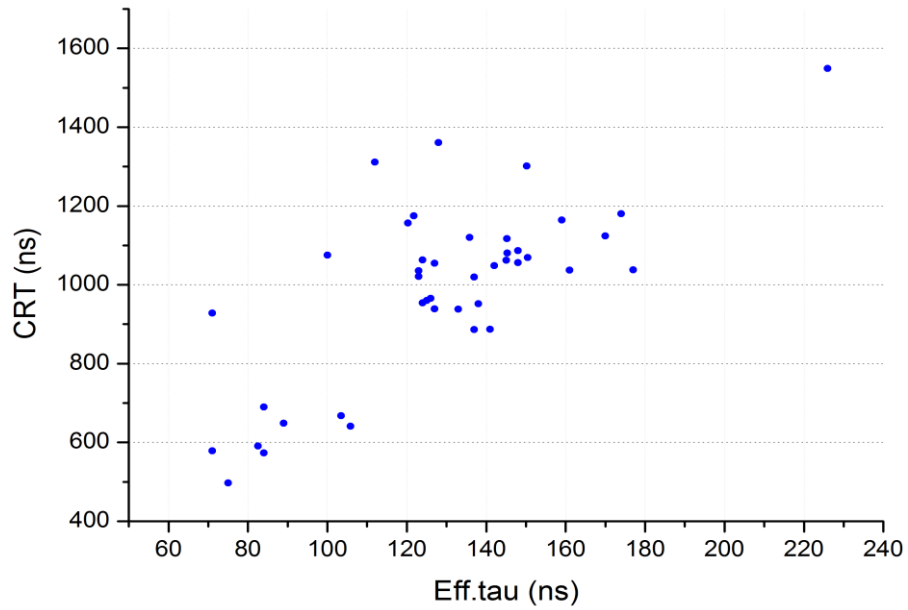


Figure 35: Relation between effective tau and CRT.

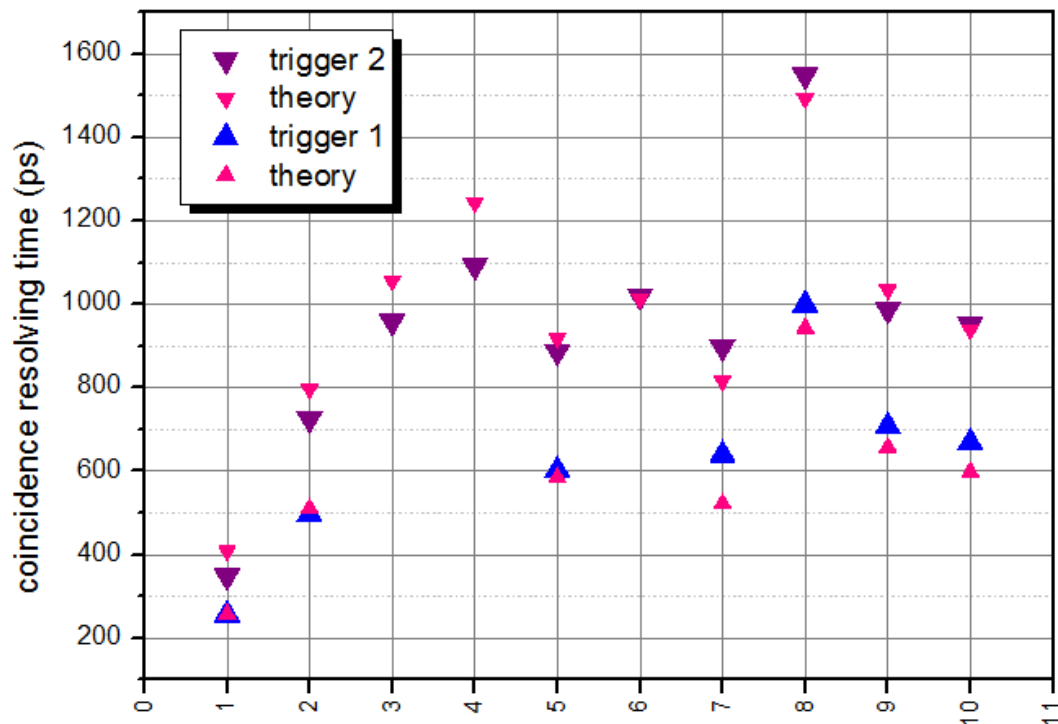


Figure 36: shows an overview of CRT measurements and results of this theory. Blue upward triangles show results for trigger level 1, purple downward triangles for trigger level 2, while the magenta triangles give the results of our CRT theory.

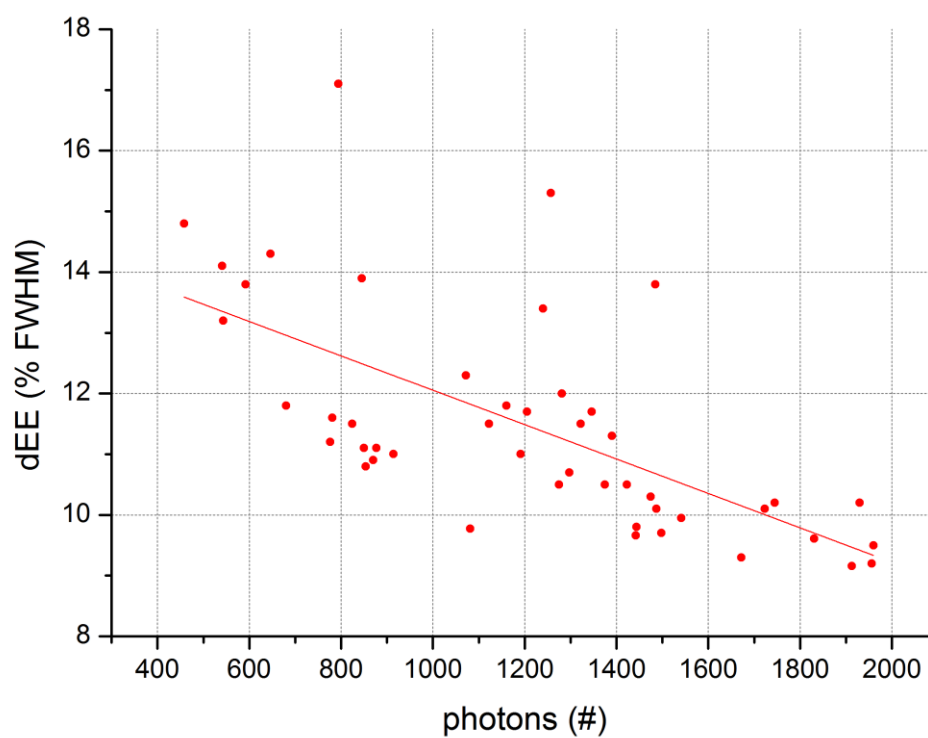


Figure 37: Relation between Energy resolution and the number of photons.

Table 6: Overview of the relevant results achieved for the sample in which the rise time was measured.

Sample	rise time (ns)	eff. decay time (ns)	photons	Trig 1 measured CRT (ps)	Trig 1 theory	Trig 2 measured CRT (ps)	Trig 2 theory
LYSO	0.57	54	1800	256	257	348	408
Furukawa	1.54	118	1903	496	510	725	796
1	2.15	137	1678	-	--	958	1056
2	2.6	141	1483	-	--	1092	1243
3	1.7	132	1723	601	585	887	918
4	1.6	128	1275	-	--	1020	1013
5	1.6	128	1183	639	522	897	816
6	2.4	179	1191	999	943	1549	1493
7	1.3	107	828	707	657	987	1034
8	1.6	123	1442	668	598	952	939

6. DISCUSSION

To achieve the goal of this project that was to identify a ceramic scintillator for TOF PET competitive with the current crystal scintillators used nowadays in PET scanners, materials to build this ceramic like Lu, Ga, Gd, Al were explored. Ce was used as an activator.

The overall results in the PMT showed that there were some samples with a faster decay than the GAGG:Ce crystal from Furukawa, which was one of the goals to achieve. It should also be mentioned that LYSO:Ce still presents a faster behavior than every ceramic tested.

The first conclusions that it is possible to take from the PMT measurement phase is the presence of a slow component/afterglow in every sample measured. This component was enhanced every time the samples were exposed to UV rays from the room lighting system. The presence of such component brought the need to create a new method to measure the fast decay component, (the first one) since the way it was measured in the beginning, directly from the software Originlab™, showed a high dependence on the slow component as well as the interval that was chosen for the fit. Since the first component of the decay time is the most important one to predict the values of the CRT, it was necessary to introduce a more accurate way to calculate this first component. That is the reason why the effective decay time was introduced (Figure 20).

The effective decay time takes into account the signal maximum right after signal rise, given in terms of the PMT measurement by $U_{PMT}(0) = N_{PMT}/\tau_d$ according to theory. With the number of photons $N_{PMT} = \int_0^{\tau_{int}} U_{PMT} dt$, measured during the integration time τ_{int} , the signal maximum is better described by an effective decay time constant $\tau_{eff} = N_{PMT}/U_{PMT}(0)$ with the integration time of the PMT signal the same as in the PDPC D-SiPM TEK measurement (645 ns) defining the number of photons N . This parameter was also very important to prove the theory to estimate the CRT values that was being developed at the same time. This effective decay time was used in every analysis of the PMT results. In Figure 22 there is the relation between the effective decay, and the first component measured directly on the software, as it is possible to see they show similar trends.

PMT measurements of powders showed a big effect of the Gallium (Ga) concentration on the ceramic. The higher the concentration of, Ga the lower are the values of decay time.

The effect of changing the Cerium (Ce) concentration also played a role. The higher the concentration of Ce the lower is the CRT. The effect of these two elements in the powders could be extrapolated to the disks or sticks, but the overall values of the decay times in disks and sticks were in general higher. The measurement of the powders presented some problems due to their complete lack of transparency and homogeneity. These two factors together generated a problem of a really low signal, sometimes near the noise level of the PMT. The trigger levels with the powders had to be adjusted to -15mV, to be possible to measure the signal. Even with this trigger level it took a longer time than with disks or sticks to get the 10000 events wanted for the analysis.

The measurement of disks brought some better insight over the general effect of the concentration of the different elements in the ceramics. This was also possible due to the high amount of measurements made with disks. In the disks the effect of Ga was also verified, so the higher the amount of Ga, the lower the decay time. But these measurements also brought a good insight into the effect of the concentration of Ce. In all the disks measured it was possible to conclude that the effective decay time, and the decay time were lower with higher values of these two elements (Figure 25, Figure 26).

The measurements with sticks showed not so obvious trends. Analyzing Figure 27 it is possible to see that the lowest effective decay time values were achieved with high Ce and high Ga, but in this case it is not as conclusive as with disks. The reason for this to happen might be due to the lower number of sticks measured compared with the number of disks. Another problem with the measurement with the sticks was the lack of transparency of some of them, causing some change in the results. The effect of the UV light in the afterglow was also very different from stick to stick. This slow component was strong enough to delay some of the measurements. When this happened the stick had to stay in the chamber until it was possible to make the measurement. The right moment to make this measurement was achieved when the current measured in the HV supply reached the 0.72mV. In the presence of afterglow this value increased until ~0.8mV.

From the PDPC TEK measurements the objective was to check four different values: CRT, light output (LO), counts and energy resolution (dE/E). The two most important parameters to observe here were the CRT and the LO.

Starting the analysis with the LO, it was verified that this parameter showed that there were some big variations in the LO with samples showing a LO below 500 optical photons at 511 keV and another ones having values near 2000 (better than LYSO and Furukawa). During these measurements it was also verified that there was a relation between the LO and the energy resolution (dE/E) at 511 keV. The higher the values of light output (LO), the better the values of the energy resolution (Figure 37). The trend of LO with Ga and Ce is shown in Figure 34. The higher values of LO were achieved with Ga=2.5, being the LO lower to higher or lower values. The effect of Ce is not that clear, but the best LO values were achieved for high concentrations of Ce, which could indicate that the best CRT and LO values would be achievable with high concentrations of Ce.

The measurements of the light output was one of the big challenges to face in this project, because there were some samples that didn't present a signal high enough to be measurable in the TEK even though it was measurable on the PMTs. The fact that the signal was not measurable in the silicon detectors, but it was on the PMT's can be due to the fact that the Philips PDPC D-SPMs are optimized to detect light in the blue region and the ceramic garnets emit light in the green region of the electromagnetic spectrum.

The CRT was another of the parameters measured in the TEK setup. This is the main parameter to identify if the project was a success, since this is the key parameter to have a TOF PET. The main goal with the CRT was to obtain better values than the ones acquired with the GAGG:Ce from Furukawa. The CRT values oscillated between 1502 ps and 572 ps. The amount of Ga in the sample was also the main factor affecting these values. The higher the amount of Ga the lower is the CRT. With the values of the CRT it was also possible to show proportionality between the values of the effective decay time and the CRT. The higher the effective decay time the higher the CRT. This trend showed that the decay time is one of the main factors affecting the CRT. Another factor with great importance to the final value of the CRT is the rise time of the samples. Due to the need of having special equipment, only available at the TU Delft (University of Delft), to make these measurements, there are only a few values available for the samples tested. Knowing this in advance, during the implementation of this project a theory to predict the values of the CRT was also tested. The formula used arises from a theoretical analysis of the CRT, based on the theory stated in [24]. The equation used to predict the CRT is the following: [25]

$$CRT \approx 3.33 \cdot \sqrt{\frac{\tau_r \tau_d}{2N}} \cdot \sqrt{Q}$$

In this prediction τ_r is the rise time, τ_d the effective decay time, measured from the PMT, N is the number of photons taken from the TEK measurements and Q refers to the trigger level. From Figure 36 it is possible to verify that our measurements are according to theory.

Another conclusion that it is possible to state from theory, and from our measurements, is how trigger levels affect the CRT. The higher the trigger levels the higher the CRT. This is easily explained by the number of photons necessary to have a valid signal. In Trigger 2 setting this number is higher, so on the overall is necessary to wait a longer time for a valid signal. The trigger level also affects the number of counts, which is lower with Trigger 1. This can also be explained by the number of photons needed to have a valid signal. Since in Trigger 1 it is only necessary to have one photon, this will lead to an increase number of triggers due to dark counts and consequently an increase of dead time of the detector and consequently to a decrease in the time which it is making valid counts.

7. CONCLUSIONS AND FUTURE WORK

During this internship I have taken over all the application relevant measurements in an industrial research and development environment, performing measurements on more than 200 different samples using PMTs, and more than 50 in the arrays.

After all of these measurements it was possible to reach some conclusions regarding the production of garnets for Time of Flight PET.

All results were analyzed considering the data from PMTs and signal height, CRT, Counts and energy resolution were measured as a function of production parameters and exact stoichiometry.

Results have shown the effect of the amount of Ga on decay time, CRT and LO. It was also possible to verify the existence of trade-off between LO and CRT: the lower the CRT the higher the LO. Regarding the effect of Ga, it was proven that the higher the amount of Ga, the lower the values of CRT, but considering the trade-off referred before, it was concluded that the ideal amount of Ga to be used should be somewhere in between 2.5 and 3. Further experiments are needed to achieve the final composition.

In every PMT measurement we have seen a secondary decay time constant in garnet samples. This secondary decay time is due to the afterglow present in every sample. The existence of this afterglow was only shown under UV light, and the effect of X-ray is still unknown. This is also another test that is necessary to make. This test assumes a greater importance because the PET scanners are used along the CT scanners, making these detectors highly exposed to X-rays.

The theory used to estimate the CRT values, based on exponential rise and decay was proven with the CRT values of our samples. In order to apply this theory to every sample it was still necessary to measure the rise time of every sample.

With this work it was also concluded that the use of the effective decay time, instead of the regular decay time directly measured in the software is more accurate.

In the overall, considering the initial objective, we can assume that the main objective of this project was achieved, with the production of ceramic garnets with a performance suitable for TOF PET. Anyway the industrial production of them is still yet to be tested.

8. REFERENCES

- [1] M. E. PHELPS, *PET: physics, Instrumentation, and Scanners*, Vol. I. California, USA: Springer, 2006.
- [2] J. Bronzino, *The biomedical engineering handbook*, Second edi. Florida: CRC Press, 1995.
- [3] J. E. Turner and W. Road, *Atoms , Radiation , and Radiation Protection*. .
- [4] F. Attix, *Introduction to radiological physics and radiation dosimetry*. Germany: Wiley-VCH, 2004.
- [5] F. R.B. and E. L.P., “Table of Radioactive Isotopes,” 2004. [Online]. Available: <http://ie.lbl.gov/toi/nuclide.asp?iZA=430399>. [Accessed: 20-Aug-2013].
- [6] M. Khalil, *Basic sciences of nuclear medicine*. London: Springer, 2011.
- [7] M. N. Wernick and J. N. Aarsvold, *Emission Tomography - The fundamentals of PET and SPECT*, 1st ed. Elsevier academic press, 2004.
- [8] M. Analoui, J. Bronzino, and D. Peterson, *Medical Imaging: Principles and Practices*. CRC Press, 2012.
- [9] G. Muehllehner and J. S. Karp, “Positron emission tomography.,” *Physics in medicine and biology*, vol. 51, no. 13, pp. R117–37, Jul. 2006.
- [10] M. Conti, “Focus on time-of-flight PET: the benefits of improved time resolution.,” *European journal of nuclear medicine and molecular imaging*, vol. 38, no. 6, pp. 1147–57, Jun. 2011.
- [11] N. J. Cherepy, S. A. Payne, S. J. Asztalos, G. Hull, J. D. Kuntz, T. Niedermayr, and S. Pimputkar, “Scintillators with Potential to Supersede Lanthanum Bromide,” pp. 873–880, 2010.
- [12] J. Y. Yeom, S. Yamamoto, S. E. Derenzo, V. C. Spanoudaki, K. Kamada, T. Endo, and C. S. Levin, “First Performance Results of Ce:GAGG Scintillation Crystals With Silicon Photomultipliers,” *IEEE Transactions on Nuclear Science*, vol. 60, no. 2, pp. 988–992, Apr. 2013.
- [13] “Knoll Glenn F. Knoll. Radiation Detection and Measurement 3rd.pdf.” .
- [14] M. Nikl, “Scintillation detectors for x-rays,” *Measurement Science and Technology*, vol. 17, no. 4, pp. R37–R54, Apr. 2006.
- [15] M. J. Weber, “Scintillation: mechanisms and new crystals,” *Nuclear Instruments and Methods in Physics Research Section A: Accelerators, Spectrometers, Detectors and Associated Equipment*, vol. 527, no. 1–2, pp. 9–14, Jul. 2004.

- [16] M. J. Weber, “Inorganic scintillators: today and tomorrow,” *Journal of Luminescence*, vol. 100, no. 1–4, pp. 35–45, Dec. 2002.
- [17] R. Mao, C. Wu, L. Dai, and S. Lu, “Crystal growth and scintillation properties of LSO and LYSO crystals,” *Journal of Crystal Growth*, vol. 368, pp. 97–100, Apr. 2013.
- [18] C. Greskovich and S. Duclos, “Ceramic Scintillators,” *Annual Review of Materials Science*, vol. 27, no. 1, pp. 69–88, Aug. 1997.
- [19] P. Is and O. U. R. Business, *Photomultiplier tubes Basics and Applications*, Third edit. Hamamatsu, 2006.
- [20] T. Frach, G. Prescher, C. Degenhardt, R. De Gruyter, A. Schmitz, and R. Ballizany, “The Digital Silicon Photomultiplier – Principle of Operation and Intrinsic Detector Performance,” pp. 1959–1965, 2009.
- [21] C. Degenhardt, G. Prescher, T. Frach, A. Thon, and R. De Gruyter, “The Digital Silicon Photomultiplier – A Novel Sensor for the Detection of Scintillation Light,” pp. 2383–2386, 2009.
- [22] R. Schulze, *PDPC-TEK User Manual*, Version 0. Aachen, Germany: Koninklijke Philips Electronics 2012, 2012.
- [23] C. Dege, “The digital Silicon Photomultiplier ,” pp. 2383–2386, Oct. 2009.
- [24] Y. Shao, “A new timing model for calculating the intrinsic timing resolution of a scintillator detector.,” *Physics in medicine and biology*, vol. 52, no. 4, pp. 1103–17, Mar. 2007.
- [25] H. Wiecezorek, “Private entry,” 2013.
- [26] Philips, “Philips SPECT scanners,” 2009. [Online]. Available: http://www.newscenter.philips.com/nl_nl/standard/about/news/press/20091127_rsna_2009_philips_persbericht.wpd.
- [27] A. D. da Silva, “Philips BrightView XCT with Astonish,” 2012. [Online]. Available: <http://clinical.netforum.healthcare.philips.com/global/Explore/White-Papers/SpectCT/A-comprehensive-solution-for-extremity-imaging>.
- [28] DESY, “PET R&D IN HAMBURG: INTRODUCTION TO PET.” [Online]. Available: <http://www-flc.desy.de/pet/intro.php>.
- [29] D. J. Kadrmas, M. E. Casey, M. Conti, B. W. Jakoby, C. Lois, and D. W. Townsend, “Impact of time-of-flight on PET tumor detection.,” *Journal of nuclear medicine : official publication, Society of Nuclear Medicine*, vol. 50, no. 8, pp. 1315–23, Aug. 2009.
- [30] H. B. L. M. Freeman, E. Clinical, and N. Medicine, *Clinical Nuclear Medicine*. Springer, 2007.

- [31] Jobwerx manufacturing network, “Philips Medical Systems nuclear medicine advancements.” [Online]. Available:
http://www.jobwerx.com/images/phg_948207_Gemini_lr.jpg.
- [32] A. E. Perkins, “Astonish TF,” *Philips Healthcare*.
- [33] D. Suson, “NaI Crystal,” 2004. [Online]. Available:
<http://physics.tamuk.edu/~suson/html/3110/>. [Accessed: 15-Aug-2013].